Chapter 8

Electrospun Nanofibrous Materials and Their Hydrogen Storage

Seong Mu Jo

Additional information is available at the end of the chapter

http://dx.doi.org/10.5772/50521

1. Introduction

The hydrogen is a clean fuel source, which produces water vapor as the only exhaust gas when it is burnt with oxygen. The chemical energy density of hydrogen (142 MJ/kg) is at least three times larger than that of other chemical fuels. When the hydrogen is electrochemically burnt using a fuel cell system, the efficiency can reach 50~60%, twice as much as the thermal process because the efficiency of the direct process of electron transfer from oxygen to hydrogen in a fuel cell system is not limited by the Carnot efficiency in [1]. However, the hydrogen volume is 3000 times higher than that of gasoline at room temperature and atmosphere because it is a molecular gas. Therefore, on-board hydrogen energy storage need compact, light, safe and affordable containment. The condensation of a monolayer of hydrogen on a solid leads to a maximum of 1.3×10^{-5} mol/m^2 of adsorbed hydrogen. For automotive applications, the US DOE required a hydrogen storage capacity of greater than 6.5 wt% and ambient temperatures for hydrogen release and moderate storage pressures for industrial applications. Hydrogen storage in carbon materials is a very attractive field since high gravimetric storage capacities may be possible owing to the low specific weight and high specific surface area of carbon. The reversibly adsorbed quantity of hydrogen on nanostructure graphitic carbon amounts to 1.5 mass% per 1000 m^2/g of specific surface area at 77 K (liquid nitrogen temperature) in [1]. On active carbon with the specific surface area of 1315 m^2/g, 2 mass% of hydrogen was reversibly adsorbed at a temperature of 77 K in [2]. Carbon materials with different nanostructures are available for hydrogen storage, e.g. carbon nanofibers (CNF), graphite nanofiber (GNF), carbon nanohorns, multiwalled carbon nanotubes (MWNT), and single-walled carbon nanotubes (SWNT).

Since the excellent 6 to 8 wt% hydrogen storage using carbon nano-materials at room temperature and with atmospheric pressure was first reported in [3], several studies on hydrogen storage using SWNT, MWNT, GNF, active carbon, and active carbon fibers etc.,

have been conducted in [4,5]. The hydrogen adsorption of 4.2 wt% (0.5-H/C) at 100 bars and at room temperature was observed using SWNT synthesized through the arc electric discharge method in [6]. A hydrogen adsorption of approximately 3 wt% at 3~100 MPa and room temperature was reported using a well-aligned SWNT bundle in [4]. The hydrogen storage of SWNTs measured using volumetric method, however, showed scattered capacities within the range of 0.03~4 wt% at room temperature because of introduction of some error during the measurement in [7,8]. As listed in Table 1, SWNTs in more accurate volumetric measurements showed low capacity within the range of 0.14~0.43 wt% and results for MWNTs and graphite powder were less than 0.04 wt% in [9]. Despite the large volume of data from studies conducted on SWNTs, MWNTs, GNFs, etc., as potential hydrogen storage materials, these data are scattered and are thus inconclusive.

Carbon nanomaterials	Sources	Evaluation Temperature/Pressure	H_2 Storage capacity
SWNT	Carbon nanotechnology Inc.	298 K / 80 bars	0.43 wt%
SWNT	MTR, Ltd (20~40% purity)	298 K / 80 bars	0.14 wt%
MWNT	ground core, Strem Chemicals, Inc	298 K / 80 bars	< 0.04 wt%
SWNT	arc-discharge	300 K /145 bars	0.2~0.4 wt%
MWNT	acetylene pyrolysis	300 K /145 bars	0.2~0.6 wt%
MWNT	arc-discharge	300 K /145 bars	2.6 wt%
aligned MWNT bundle	ferrocene pyrolysis	300 K /145 bars	1.0~3.3wt%
aligned MWNT bundle	ferrocene/acetylene pyrolysis	300 K /145 bars	3.5~3.7wt%
GNF	acetylene pyrolysis	-	2.4 wt%
GNF	hexane/ferrocene pyrolysis	298 K /100 bars	1.29~3.98 wt%
Commercial ACF	A-20(Osaka Gas Chemicals Co. Ltd) /FT300-20(Kuraray Chemical Co., Ltd)_	298 K / 80 bars	0.35~0.41 wt%
vitreous carbon	80-200μm, 99.5% purity (Goodfellow Cambridge, Ltd.)	298 K / 80 bars	< 0.04 wt%
Graphite powder	200μm, 99.997% purity (Goodfellow Cambridge Ltd.)	298 K / 80 bars	< 0.04 wt%

Table 1. The hydrogen storage capacities of several carbon nano-materials evaluated by using the PCT and gravimetric method.

Typical carbon materials, such as active carbon, active carbon fiber, and graphite powder, were also investigated as potential materials for hydrogen storage. Purified SWNT (285 m^2/g) and saran carbon (1600 m^2/g) with a high BET surface area were also reported to have a hydrogen adsorption of approximately 0.04 and 0.28 H/C, respectively, at 0.32 MPa and 80 K in [5]. Large hydrogen adsorption was also observed by a micro porous zeolite and active carbons at 77 K under atmospheric pressure in [10]. In the case of highly porous carbon (AX-21 carbon), very high hydrogen adsorption of 5.3 wt% (0.64 H/C) was observed at 77 K and 1 MPa in [11]. However, active carbon materials with very high surface areas showed very low capacities at room temperature. This may be due to the very low levels of the effective pore size for hydrogen storage in spite of their high surface areas. The hydrogen storage capacity of materials surface greatly depended on the adsorption potential energy between the materials and hydrogen molecules. But too high adsorption potential energy may give to irreversible storage with chemisorptions of hydrogen molecule. The potential fields from opposite walls may overlap so that the attractive force acting on hydrogen molecules is greater than that on an open flat surface. Therefore, in micro porous carbon materials the pores with a width not exceeding a few hydrogen molecules may be more effective pores for hydrogen storage because of the dynamic diameter of hydrogen molecule with 0.41 nm, in [1].

TiO_2 nanotubes could reproducibly store up to about 2 wt% H_2 at room temperature and 60 bars in [12]. However, only 75% of the H_2 is physisorbed and can be reversibly released upon pressure reduction. Approximately 13% is weakly chemisorbed and can be released at 70 °C as H_2, and 12% is bonded to oxide ions and released only at temperatures above 120 °C as H_2O. The sorption of hydrogen between the layers of the multilayered wall of nanotubular TiO_2 was also investigated in the temperature range of -195 to 200 °C and at pressures of 0 to 6 bar and it got a 1~2.5 wt% hydrogen sorption at 1 bar and temperatures in the range 80 to 125 °C, in [13]. The hydrogen storage capacity of 0.83 wt% using ZnO nanowires with the mean diameter of 20 nm was found under the pressure of about 3.03 MPa and at room temperature, and about 71% of the stored hydrogen can be released under ambient pressure at room temperature, in [14]. And also hydrogen storages using MoS_2 nanotube and TiS_2 nanotube were investigated in [15,16]. So we need the study on the effective pore size of materials with appropriate adsorption potential energy for hydrogen storage at room temperature rather than large surface area of materials.

Carbon fibers have been used in a variety of fields as high-performance and functional materials. Woven or nonwoven carbon fibers are used as absorbed materials because of better adsorption capacity than conventional activated granular and powder carbon materials. They are being applied to gas separation and liquid adsorption. Saran carbons showed higher the hydrogen storage capacity than that of other active carbon materials, in [5]. Poly(vinylidene fluoride) (PVdF) also can be used in obtaining meso porous carbon similar to saran polymers, in [17]. The carbonization of PVdF can also produce a polyacetylene or carbyne structure and its pore size may be smaller than that of saran carbon due to the small size of the fluorine atom. Nano-sized fibers may be more helpful in obtaining carbon materials with a well-defined pore structure compared to the

carbonization of micro-sized polymer fibers. Because thinner fibers are expected to be more desirable for those separation and adsorption applications, there has been growing interest in electrospinning for producing ultrafine fibers.

The recent electrospinning process for polymer or metal oxide sole gel solutions is a powerful method for producing ultrafine fibers within the range of a few to a few hundred nanometers in diameter, core-shell nanostructure nanofibers, etc., which cannot be easily obtained using traditional methods. There is a growing interest in the electrospinning process of polymer or metal oxide sol-gel solution because of their several potential applications such as ultrasensitive gas sensors, polymer electrolytes for lithium ion polymer battery, dye-sensitized solar cell etc., in [18~22]. Thus, such electrospun polymeric nanofibers can be used as effective precursors for carbon nanofibers. In addition, a transition metal would promote carbonization and graphitization of polymeric precursor, which was verified for Kapton films by various research groups, in [23~25]. Recent reports showed the effects of a transition metal on the carbonization behavior of the electrospun polyimide nanofiber, PAN nanofibers and PVdF nanofibers, resulting in graphite nanofiber (GNF), in [26,27]. And also electrospinning of metal oxide sol-gel solution provide metal oxide nanofibers with various morphologies after calcinations. They are also expected to have some hydrogen storage because of higher adsorption potential energy between the metal oxide materials and hydrogen molecules although they had much lower surface area than those of electrospun polymer based carbon nanofibers.

In this chapter, the preparation of carbon nanofibers, graphite nanofiber, and metal oxide nanofibers such as titanium oxide and lithium titanate nanofiber through heat-treatment of electrospun precursor nanofibers, their structural properties such as surface area and pore size, and morphologies were investigated. And their hydrogen storage capacities discussed with their pore size and surface area.

2. Results and discussion

2.1. Morphology and crystalline structure of CNFs, GNFs, and lithium titanate nanofiber

Polyacrylonitrile (PAN) typically has been used for preparation of carbon fiber with high performance. Carbonizations of PVdF or saran polymers also give to meso porous or micro porous carbon materials. Ultrafine structure of electrospun PVdF nanofibers is expected to be suitable for the formation of pores which are effective for hydrogen adsorption, compared to PVdF films or microfibers. So, micro porous carbon nanofibers as hydrogen storage materials were prepared through the carbonization of as-electrospun PAN and PVdF nanofibers. As-electrospun PAN or PVdF-based nanofibers were prepared from the typical electrospinning of the polymer solution containing several contents of iron (III) acetylacetonate (IAA) on the weight of the polymer as a catalyst for graphitization. Carbon nanofibers (CNF) and graphite nanofiber (GNF) were prepared from carbonization after stabilization of them, in [28~31].

Firstly polyacrylonitrile (PAN) solutions for electrospinning were prepared by dissolving PAN (Mw 150,000, polyscience) in N,N′-dimethylacetamide. The PAN solutions contained 0 wt%, 2 wt%, 5wt%, and 7.5 wt% of iron (III) acetylacetonate (IAA) on the weight of the polymer as a catalyst for graphitization. As-electrospun PAN-based nanofibers were stabilized by heating them at a rate of 1 °C/min up to 260 °C, and by holding them for 2 hrs under air atmosphere. Carbonization was performed at a given temperature within the range of 900 to 1500 °C under nitrogen atmosphere. The samples were kept for 1 hr sequentially at 400 and 600 °C and then heated up to final temperature at a rate of 3 °C/min. As-electrospun PVdF nanofibers were also obtained from electrospinning of 11 wt% PVdF solution (Kynar 761) in acetone/N,N′-dimethylacetamide (=7/3, wt. ratio) mixture. They were slightly dehydrofluorinated (DHF) in the methanol/ N, N′-dimethylacetamide (=9/1 wt. ratio) solution containing 10 ml of 1,8-diazabicyclo[5.4.0] undec-7-ene (DBU) at 50 °C for 5 hours. They were also highly dehydrofluorinated in the methanol/DBU (=1/2 wt. ratio). A PVdF solutions for GNFs were prepared by dissolving 11 wt% of PVdF in 100 ml of acetone/N,N′-dimethylacetamide (=7/3, wt. ratio) mixture containing 25 ml of 1,8-diazabicyclo[5.4.0] undec-7-ene for partial dehydrofluorination and also contained 5.5 wt% of IAA based on the weight of the polymer as a catalyst for graphitization. As-electrospun PVdF nanofibers for GNFs were chemically dehydrofluorinated with a 4 M aqueous NaOH solution containing 0.25 mmole of tetrabutylammonium bromide at 70 °C for 1 h. Carbonization was performed to induce micro pore structures without a further activation process at a given temperature within the range 800~1800 °C under a nitrogen atmosphere. The samples were heated at a rate of 3 °C/min and were maintained for 1 h at the final temperature.

Figure 1 shows the SEM images of electrospun PAN- and PVdF-based CNFs. In the case of as-electrospun PAN-based nanofiber with a diameter of about 90 nm the fiber diameter hardly changed during the carbonization at 1300 °C, while that with a diameter of about 240 nm remarkably shrank to 110 nm and showed roughened surfaces. Solvent evaporation during the electrospinning process greatly has an effect on internal structure of the resulting PAN nanofibers. Thin fiber is denser and has a higher orientation than thick fiber because it is formed at a much higher draw ratio and with a much faster solvent evaporation during the electrospinning process. Oxidation and carbonization of the above as-electrospun PAN nanofibers were carried out under a tensionless condition or with a slight tension. Therefore, the dimensions of dense, highly oriented ultrathin fibers are thought to hardly change during carbonization and the PAN-based CNFs showed very smooth surfaces. In the case of as-electrospun PVdF nanofibers, it is also necessary to make the nanofibers infusible to maintain their fibrous shape through dehydrofluorination (DHF) treatment before the carbonization. The effect of DHF treatment in the carbonization of PVdF polymer has been reported in previous studies, in [17]. The structure of the PVdF-based CNFs greatly depends on the DHF condition, in [30]. The carbon nanofibers carbonized after a high DHF treatment had very smooth surfaces and dense, nonporous structures in Figure 1(c), while slightly DHF treatment gave to the micro porous carbon nanofibers with granular-shaped surfaces, and with an internal structure consisted of 20 to 30-nm carbon granules after carbonization

at above 800 °C, as shown in Figure 1(d). The pore structure became dense with the increase of carbonization temperature, indicating the formation of micro pores at higher temperature. The slight DHF treatment of PVdF nanofibers induced inhomogeneous structures consisting of the DHF-treated, amophorous region and the non-reacted crystalline region. The non-reacted crystalline region melted at a high temperature while the dehydrofluorinated region maintained its fibrous shape during the carbonization. The onset temperature and the amount of volume reduction during carbonization differed between the non-reacted and reacted regions. Thus, relatively large pores were produced between these regions.

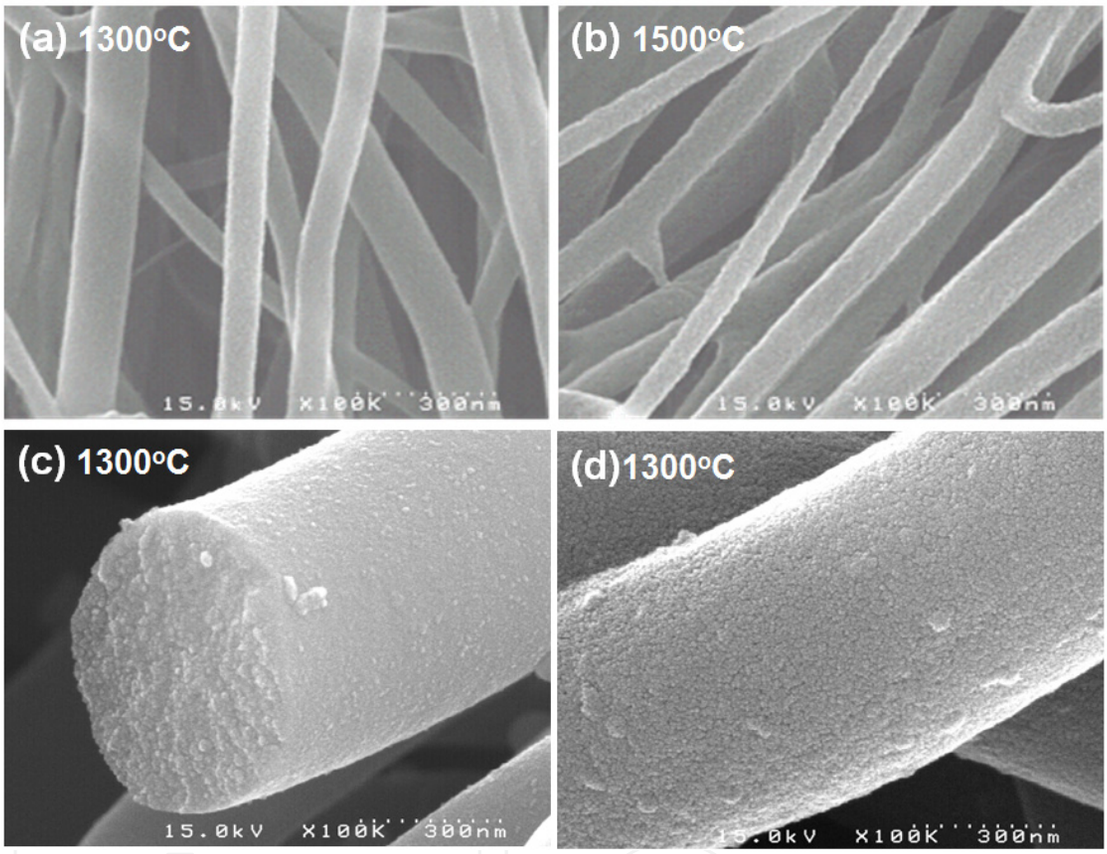

Figure 1. SEM images of carbon nanofibers prepared through carbonization of electrospun PAN nanofibers (a), (b), and PVdF nanofibers after (c) high DHF, (d) low DHF- treatment. in [28~30] (*These data were reproduced under permissions of The Polymer Society of Korea and Cambridge University Press*)

As shown in Figure 2, the PAN-based CNFs had disordered, amorphous carbon structures with d_{002}>0.37 nm, and had broad peaks structures in the XRD regardless of the carbonization temperature. The PVdF-based CNFs also showed disordered carbon structures in the XRD and Raman spectra regardless of the carbonization temperature. The CNFs prepared after low DHF treatment were expected to have higher surface areas than those prepared after high DHF treatment. Their high surface areas are thought to be due to their micro porous granular surfaces. However, this does not indicate high hydrogen storage capacity because micro pores with a width not exceeding 1 nm are thought to be much more effective for hydrogen storage when compared to the kinetic diameter of hydrogen molecule sizes of about 0.41 nm.

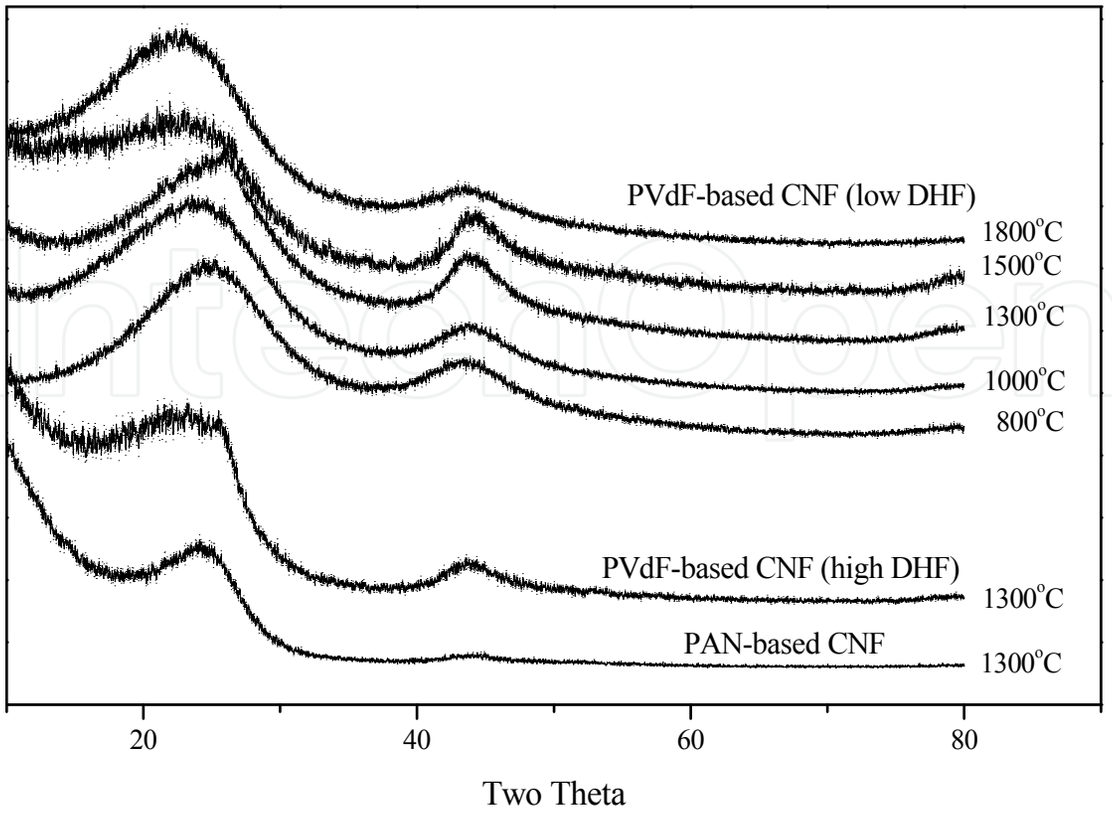

Figure 2. XRD patterns of (a) the PAN- and (b) the PVdF-based CNFs. in [28] (*These data were reproduced under permissions of The Polymer Society of Korea*)

Catalytic graphitization using volatile hydrocarbon fractions during the carbonization may be helpful in increasing the carbon yield and in forming effective ultra micro pores for hydrogen storage. For these purpose, as-electrospun PAN and PVdF nanofibers containing IAA were carbonized to induce catalytic graphitization within the range 800~1800 °C under a nitrogen atmosphere. PAN based graphite nanofibers (GNF) with a diameter of 150-300 nm were prepared by carbonization at 900~1500 °C after stabilization of as-electrospun PAN nanofibers containing 2, 5, and 7.5 wt% of IAA at air atmosphere, respectively. Figure 3 and 4 shows SEM and TEM images of PAN-based GNF. White spots were observed on the surface of the GNF fibers (1100 °C), indicating the development of graphite crystal structures centered on the Fe catalyst. This catalytic graphitization was accelerated at above 1300 °C. The TEM image around the white spot on the surface of the GNF showed a well-ordered graphite structure similar to natural graphite.

In the case of PVdF-based GNF, a notable grainy structure was observed on the surface and cross-section of the GNFs. The partial dehydrofluorination of PVdF nanofibers induced inhomogeneous structures consisting of a dehydrofluorinated amorphous region and an non-reacted crystalline region. Therefore, carbonization of them produced porous GNFs with a high surface area due to their porous granular surface. Figure 5 shows SEM and TEM images of PVdF-based GNFs. Clusters of Fe catalyst and the development of graphite structures centered on the Fe catalyst are clearly observed in TEM images of PVdF-based GNFs. The size of the Fe catalyst is from a few tens to a few hundreds of nanometers.

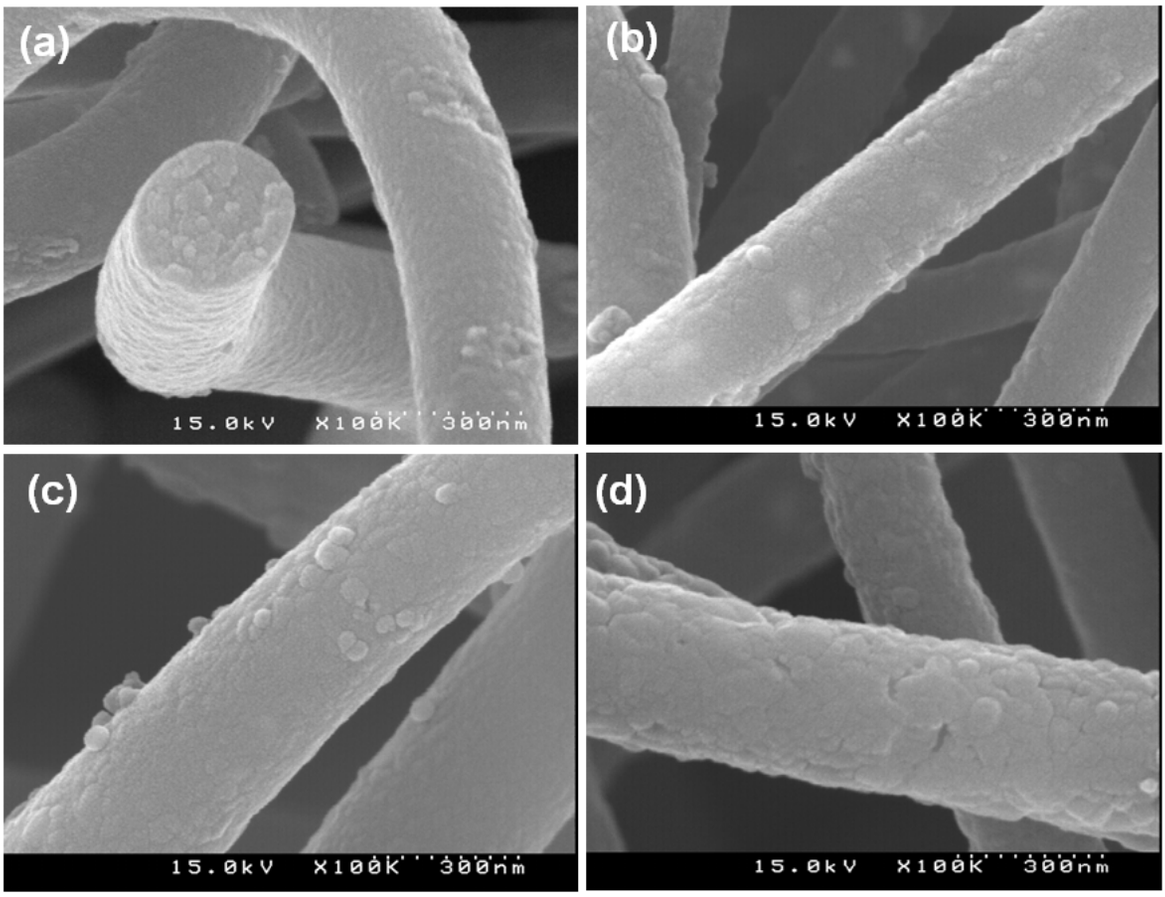

Figure 3. SEM images of the GNFs prepared from electrospun PAN nanofibers containing IAA 2 wt% ; carbonization; (a) 900°C (b) 1100°C (c) 1300°C (d) 1500°C. in [28] (*These data were reproduced under permissions of The Polymer Society of Korea*)

Figure 6 and 7 shows XRD patterns of PAN and PVdF-based GNFs. The catalytic graphitization of electrospun PAN nanofibers intensively started to proceed from 900 °C, while PVdF nanofibers intensively started to proceed from 800 °C. The sharp peaks in the PAN-based GNF at 1100 °C were observed at around 26° (002) and 42-46° (100), respectively. New peaks also appeared at 35° and 50°, corresponding to Fe_3O_4. In the case of PVdF-based GNFs, the GNFs at 800 °C show sharp peaks at approximately 26° and 44°, corresponding to the diffraction of the (002) plane and (100)/ (101) of the graphite structure, respectively. The presence of the (112) peak at 83° is also indicative of a graphite structure. The intensities of these peaks increased and sharpened with the carbonization temperature. New peaks also appeared at 36° and 48°, corresponding to Fe_3O_4. It was assumed that IAA was converted into Fe_3O_4 *via a*-FeO(OH) during carbonization, and that the reduction of Fe_3O_4 at above 800~900 °C resulted in the production of the α-Fe catalyst to be able to induce the graphitization reaction of the PAN or PVdF based nanofibers. In the case of the PAN-based GNF prepared at above 1300 °C, most of the Fe_3O_4 transformed to the α-Fe. As shown in Figure 6, the PAN-based GNFs using higher contents of IAA and higher carbonization temperature obviously showed α-Fe peak at around 42-44° (110) and 65° (200). The PVdF-based GNF prepared at 1500 °C obviously showed α-Fe peaks at approximately 42~44° (110)

and 65° (200). Since the GNFs, however, did not entirely have this graphite structure, the d_{002} of PAN-based GNFs and PVdF-based GNFs were almost 0.34 nm and in the range 0.333~0.343 nm, respectively. The net structure of these GNFs consists of a graphite-like structure, which forms a turbostratic-oriented graphite layer. Generally, this type of structure has been obtained from carbonization of rigid polymers such as Kapton imides, in [32]. However, the electrospun thermoplastic nanofibers also transformed to form a well ordered graphite structure similar to natural graphite through catalytic graphitization during carbonization. Single hexagonal crystal graphite shows a Raman active peak at 1582 cm^{-1} (G mode) and a band around 1357 cm^{-1} can be attributed to the D mode of disorder induced scattering, which is due to imperfection or lack of hexagonal symmetry in the carbon structure. A wide Gaussian band (M mode) is considered to represent an amorphous carbon contribution. $L_a=4.2(I_G/I_D)$ in Raman spectra reflects the crystallite planar size of the graphite structure. As listed in Table 2, the Raman spectra of the PAN-based GNFs show that the relative intensity of the G band (1580 cm^{-1}) over the D band (1360 cm^{-1}) increased with the increase of the carbonization temperature. *La* (nm) greatly increased to 4.1 nm (900 °C), 4.75 nm (1100 °C), and 6.54 nm (1300 °C). As shown in Figure 8, the I_G/I_D of the PVdF-based GNFs also rapidly increased with increasing carbonization temperature. L_a (nm) greatly increased from 4.32 nm (800 °C) to 72.5 nm (1800 °C) with increasing carbonization temperature, in [31].

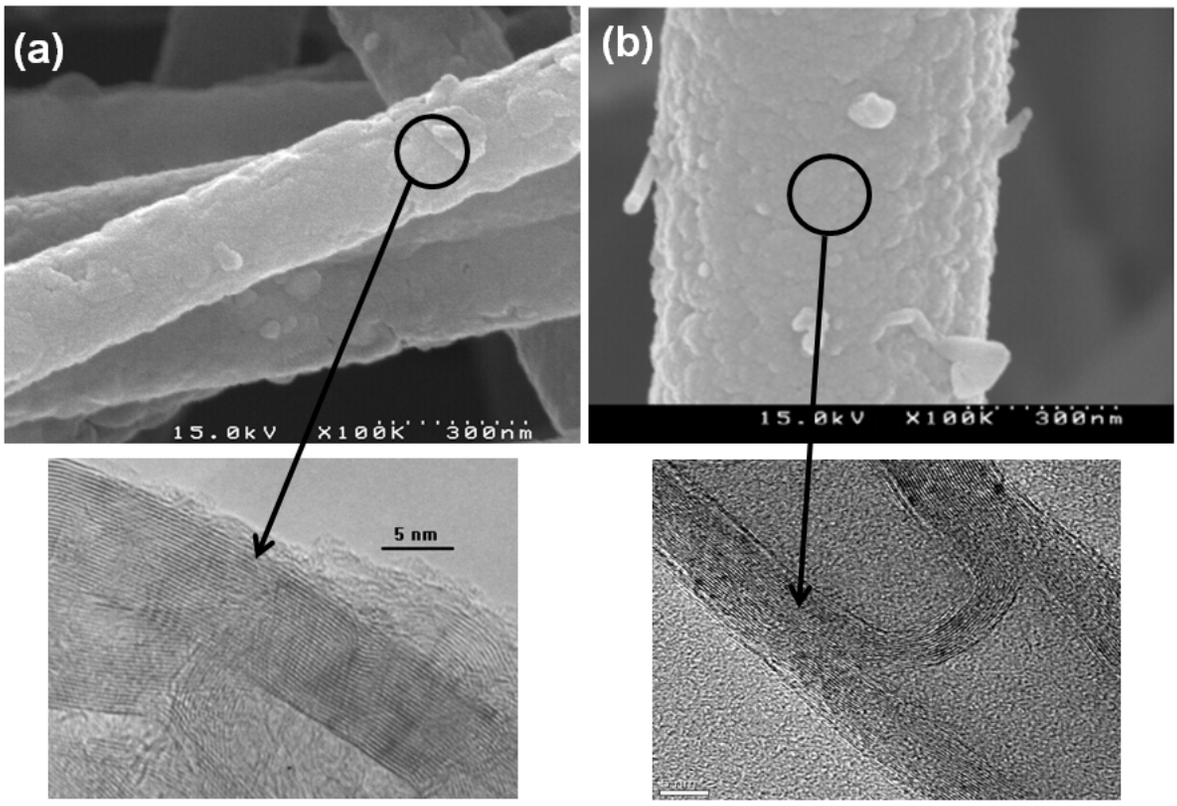

Figure 4. SEM and TEM images of the GNFs prepared through carbonization of electrospun PAN nanofibers containing IAA (a) 5 wt%, (b) 7.5 wt%. in [28] (*These data were reproduced under permissions of The Polymer Society of Korea*)

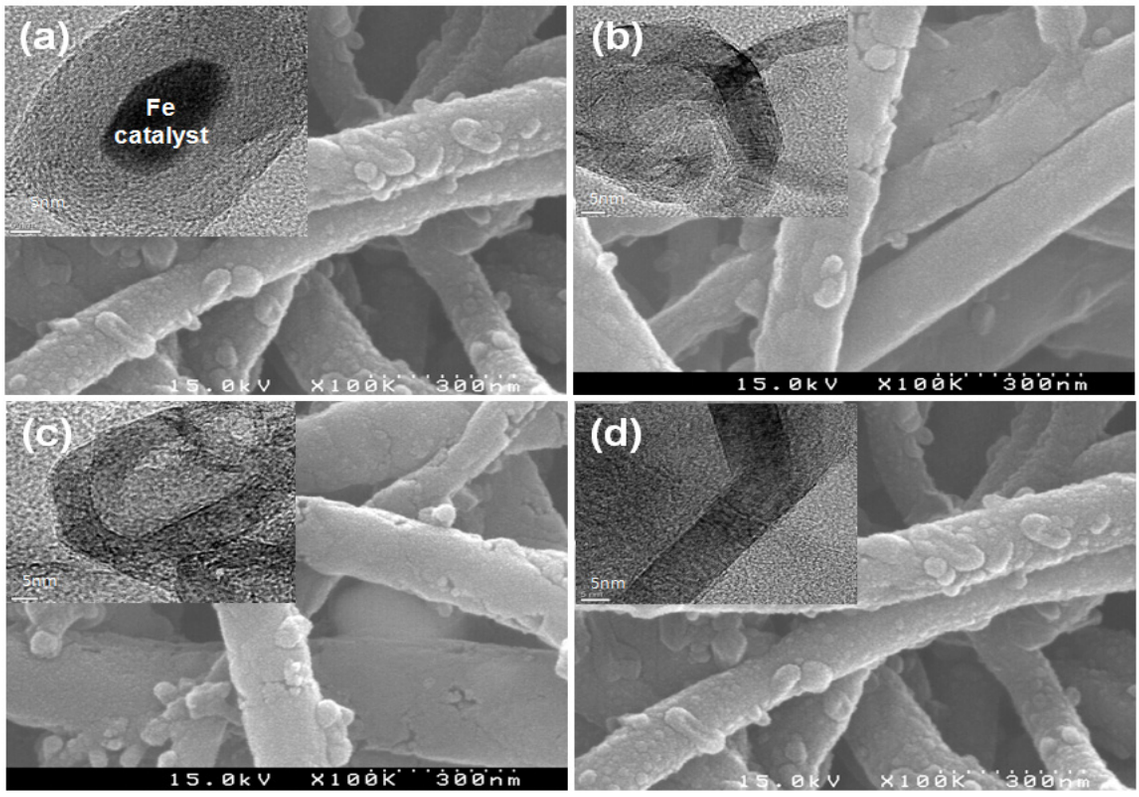

Figure 5. SEM and TEM images of the GNFs prepared through carbonization of electrospun PVdF nanofibers containing IAA 5.5 wt%. (a) 800°C; (b) 1000°C; (c) 1500°C; and (d) 1800°C. in [31] (*These data were reproduced under permissions of Elsevier)*

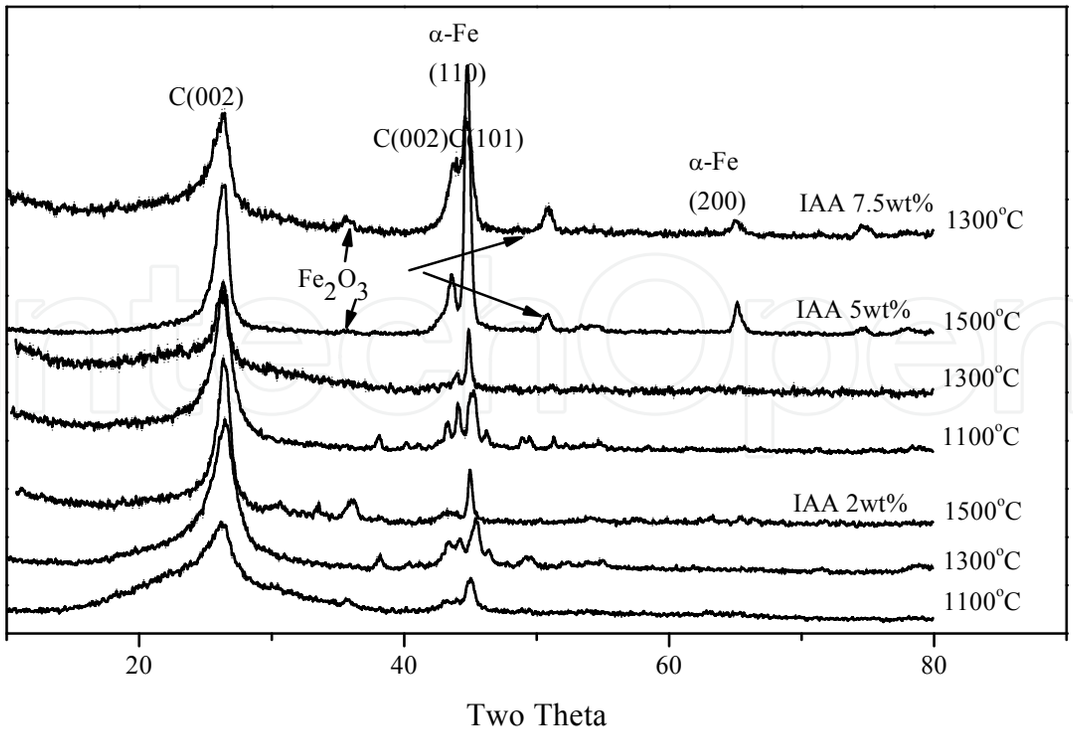

Figure 6. XRD patterns of the PAN-based GNFs. in [28] (*These data were reproduced under permissions of The Polymer Society of Korea*)

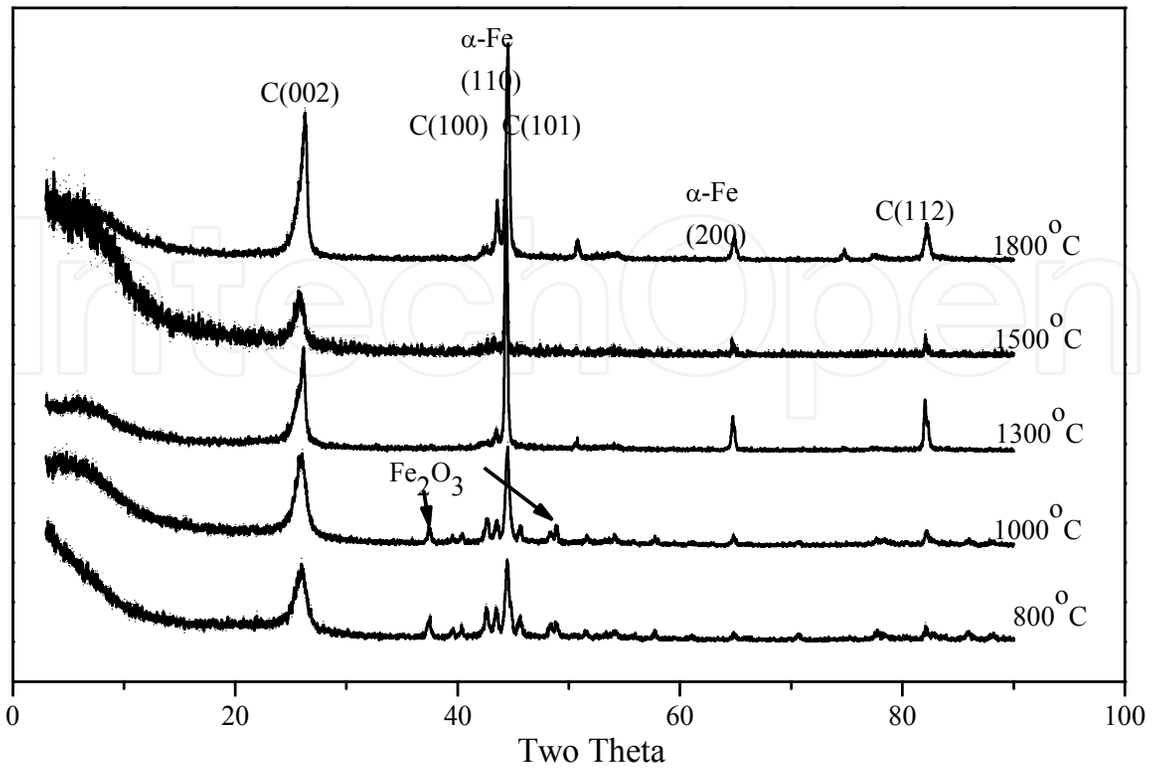

Figure 7. XRD patterns of the PVdF-based GNFs. in [31] (*These data were reproduced under permissions of Elsevier)*

Samples	Carbonization Temperature(°C)	XRD		Raman
		2 theta(°)	$d_{002}(nm)$	$L_a(nm)^a$
PAN-based CNF	1300	25.98	> 0.370	-
PAN-base GNF	900	25.90	0.344	4.10
	1100	26.10	0.341	4.75
	1300	26.12	0.341	6.54
PVdF-based GNF	800	26.11	0.341	4.32
	1000	25.96	0.343	4.83
	1300	26.12	0.341	7.50
	1500	26.28	0.339	10.9
	1800	26.27	0.333	72.5

a : L_a *(Raman)* = 4.4 (I_G/I_D)

Table 2. The (002) spacing values and in-plane sizes of small graphite crystals, L_a, of electrospun PAN- and PVdF-based graphitic carbon nanofibers. in [31] (*These data were reproduced under permissions of Elsevier)*

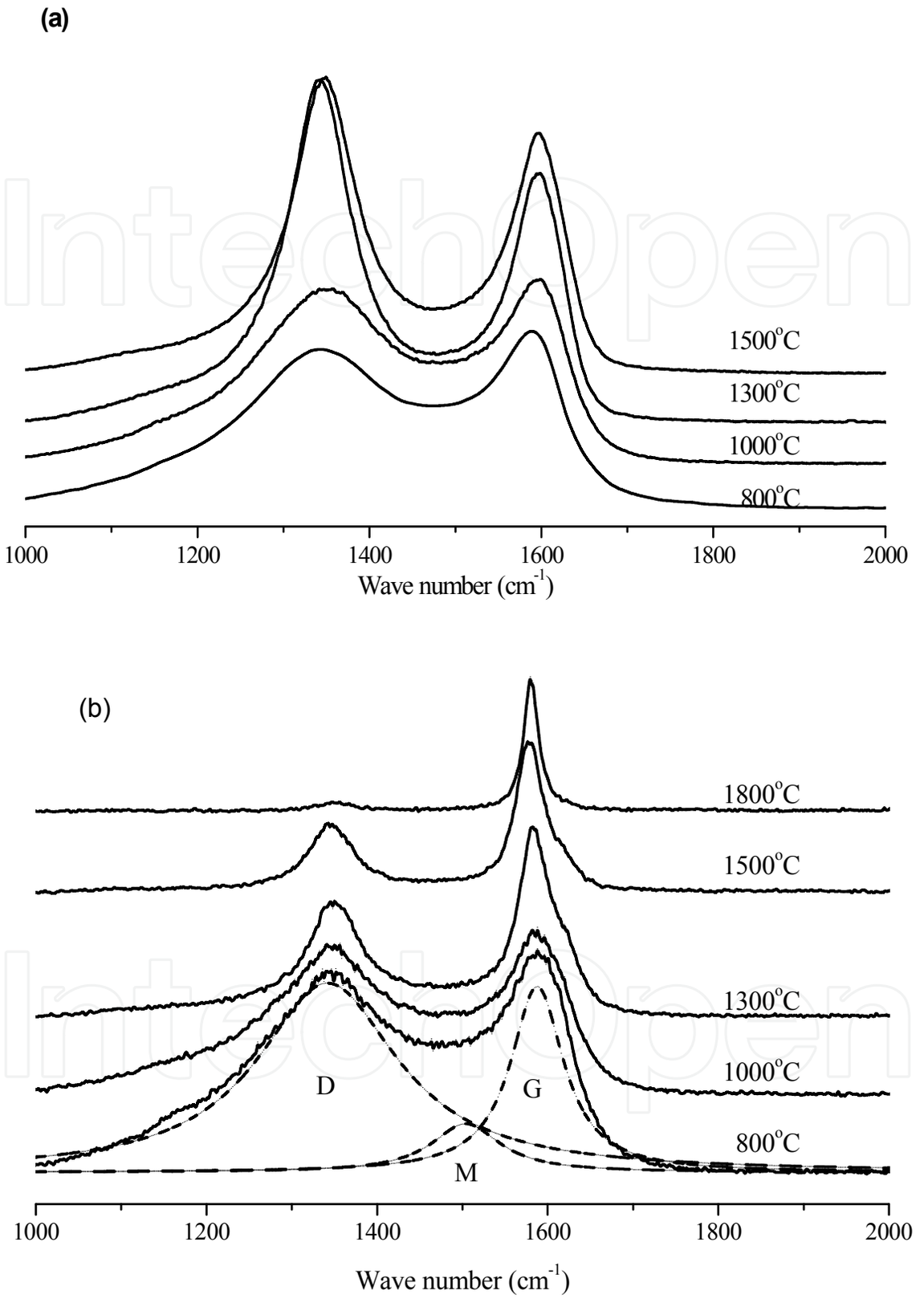

Figure 8. Raman spectra of the PVdF-based (a) CNFs and (b) GNFs at several carbonization temperatures. in [31] (*These data were reproduced under permissions of Elsevier)*

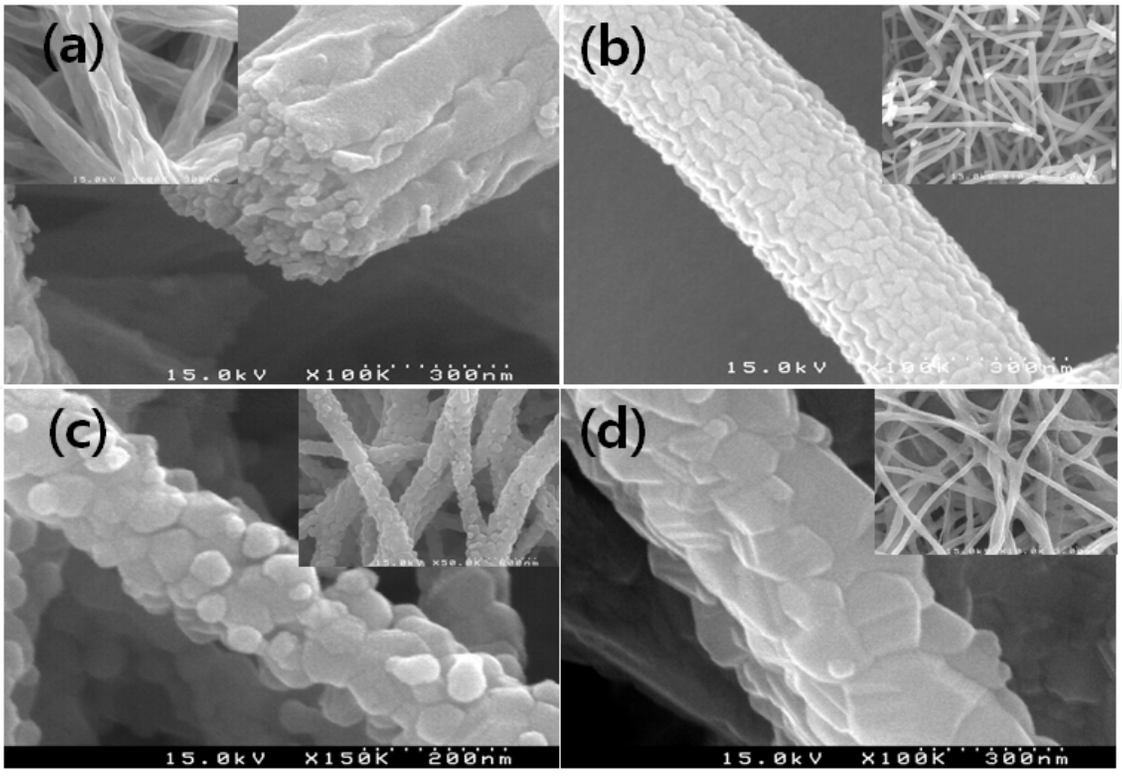

Figure 9. SEM images of (a) electrospun TiO_2 nanofiber after calcinations at 450°C, and electrospun $LiTi_2O_4$ nanofibers after calcinations at (b) 450°C (c) 600°C, and (d) 700°C.

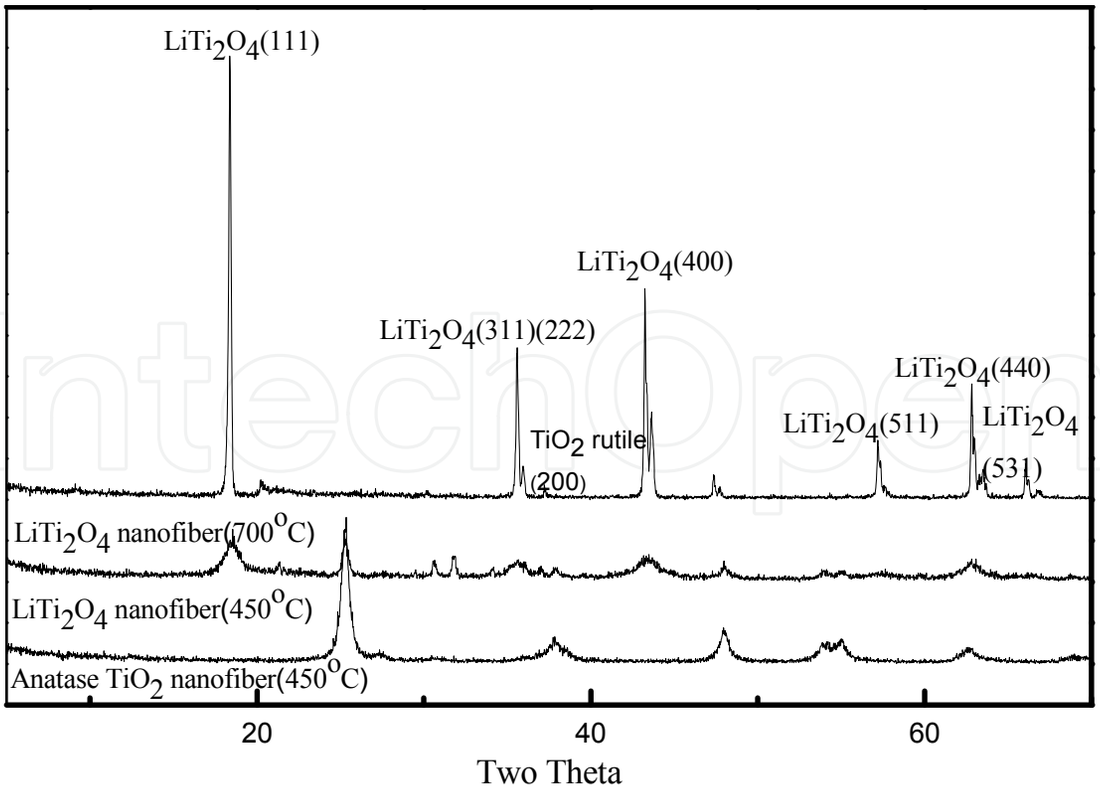

Figure 10. XRD patterns of electrospun TiO_2 nanofiber (a) and $LiTi_2O_4$ nanofibers after calcinations at 450°C and 700°C.

TiO_2 nanofiber was also prepared from typical electrospinning of a mixture solution of titanium tetraisoproxide and polyvinyl acetate (PVAc, Mw 500,000) in N, N'-dimethylacetamide (DMF). As-electrospun TiO_2/PVAc nanofiber was calcined at 450°C to completely remove the PVAc component by thermal decomposition and to give to TiO_2 nanofiber. As shown in Figure 9, the resulting TiO_2 nanofiber showed a smooth surface and internal structure composed of 20- to 50-nm TiO_2 granules. Figure 10 indicated this TiO_2 nanofiber was composed of typical anatase crystalline. Lithium titanate nanofiber was also prepared by electrospinning using a mixture of $LiNO_3$ and titanium tetraisoproxide (1:2 mole ratio) instead of titanium tetraisoproxide similar to preparation of TiO_2 nanofiber. As-electrospun lithium titanate/PVAc nanofibers were calcined at 450°C, 600°C, and 700°C to remove the PVAc component by thermal decomposition and to give to lithium titanate nanofibers. As shown in Figure 9, the lithium titanate nanofiber calcined at 450 °C showed lots of wrinkled structure in the surface and it looked like the surface composed of 20 to 60-nm nanorods. Crystalline size of lithium titanate was increased with increase of calcinations temperature. The lithium titanate nanofibers calcined at 600 °C and 700 °C showed the fibrous morphology composed of lithium titanate granules. These lithium titanate nanofibers calcined at above 450°C were typical crystalline structure of $LiTi_2O_4$ as show in Figure 10, in [33, 34].

2.2. Specific surface area and pore structure

The electrospun PAN-based CNFs showed the typical adsorption curves very similar to that of nonporous carbon in the nitrogen gas adsorption-desorption isotherms, while the PAN-based GNFs showed the typical curve of micro porous carbon in addition to a hysteresis loop that indicates existence of the meso pore, as shown in Figure 11. The PAN-based CNFs and GNFs had low surface areas within the range of 22~31 m^2/g and 60~253 m^2/g, respectively, as listed in Table 3. The surface areas of PAN-based GNFs were much higher than the CNFs, but they decreased with increase of carbonization temperature and increased with increase of IAA content. Although this could not be fully explained at present, it may be due to the surface roughness and inhomogeneous structure of the GNFs, which resulted from the induction of the metal catalyst in the GNFs. But they still had much lower surface area compared to common active carbon. Commercial active carbons and active carbon fibers generally have very high surface areas of above 1000 m^2/g, and SWNT also has a surface area of a few hundred m^2/g. They had low storage capacities, however, within the range of 0.35-0.41 wt%, at room temperature, in [9]. So, high hydrogen adsorption by PAN-based CNFs and GNFs with very low surface area may not be expected. However, if they have effective pores for hydrogen storage when compared to hydrogen molecule sizes of about 0.41 nm, they may show high hydrogen adsorption. The electrospun PAN-based GNFs showed the adsorption curves very similar to that of meso porous carbon in the nitrogen gas adsorption-desorption isotherms in spite of their low surface area and also they had micro pores unlike those in the CNFs in the nitrogen gas adsorption-desorption isotherms. In the case of the PAN-based CNFs the change of the pore volumes with increase of carbonization temperature did not show because of their very low surface area. The micro

pore volumes and meso pore volumes of the PAN-based GNFs, however, decreased with increase of carbonization temperature.

The electropun PVdF-based CNFs prepared after a slight DHF-treatment showed typical curves of micro porous carbon in the nitrogen gas adsorption-desorption isotherms. They showed high surface areas of 414~1300 m^2/g. BET surface area rapidly decreased with increase of carbonization temperature, as shown in Table 3**.** Micro pore volume at 1500 ^oC greatly decreased while meso pore volume continuously increased with an increase of carbonization temperature. However, the PVdF-based CNF at 1800 ^oC showed a very high surface area of 1300 m^2/g and a high volume (1.767 cm^3/g) of only ultra- or super micro pores. The PVdF-based CNFs prepared after high DHF-treatment showed very low surface area and adsorption curves similar to those of nonporous carbon in nitrogen gas adsorption-desorption isotherms. They did not have the micro pores. In the case of PVdF-based GNF nitrogen adsorption–desorption isotherms were the type II showing a hysteresis loop that indicates the existence of meso pores, as shown in Figure 11**.** They showed high surface areas of 377~473 m^2/g but still have low surface areas compared to typical active carbon. The BET surface area and micro pore volume decreased with increasing carbonization temperature, as listed in Table 3. Decreases in the surface area and micro pore volume are thought to be due to densification of the porous structure with increasing carbonization temperature. Nitrogen adsorption–desorption isotherms for the $LiTi_2O_4$ nanofiber calcined at 450 ^oC were also the type II showing a hysteresis loop that indicates the existence of meso pores, as shown in Figure 10. However, the TiO_2 nanofiber and the $LiTi_2O_4$ nanofibers calcined at 450 ^oC have very low surface are of about 50 m^2/g, as listed in Table 4. The surface area of the $LiTi_2O_4$ nanofibers calcined at 700 ^oC decreased with increase of crystalline size.

The pores in carbon materials are classified by their size into macro pores (> 50 nm), meso pores (> 2-50 nm), and micro pores (< 2 nm) according to IUPAC. Micro pores are further divided into super micro pores with a size of 0.7~2 nm and ultra micro pores of less than 0.7 nm, in [35]. Unfortunately, it is difficult to exactly analyze the ultra micro pore size distribution and volume in porous carbon through the nitrogen gas adsorption-desorption isotherms measurement when compared to the kinetic diameter of hydrogen molecules. In the case of direct observations of pores on the surface of carbon materials by scanning tunneling microscopy (STM/AFM), the problem is how to differentiate the pores from other surface defects, such as depressions and trenches. The net ultra micro pore volume of carbon material cannot obtain from the pore analysis of small area on the surface by STM. The oxidation and carbonization of PAN precursor fiber for making carbon fiber usually accompany with the release of NH_3, HCN, N_2 gases, etc., resulting in the formation of pores within the carbon fiber structure, in [35]. So the preparation of carbon fiber with high tensile strength requires the removal of pore structure by heat treatment at high temperature. The carbonization of the electrospun PVdF nanofibers is also usually accompanied by the release of HF, H_2, F_2 and other gases, resulting in the formation of pores within the carbon fiber structure. In addition, micro and meso pores

are generated through the carbonization of PVdF nanofibers after partial dehydrofluorination. The calcinations of as-electrospun lithium titanate/PVAc nanofibers or TiO_2/PVAc nanofibers may also produce the pore structure by evaporation of thermally decomposition product of PVAc. Therefore, we assume the generation of ultra micro pores and super micro pore during the carbonization and calcinations of the electrospun polymeric nanofibers and metal oxide nanofiber precursors. These pore structures became dense with the increase of carbonization temperature. Therefore, increase of carbonization temperature might bring out the increase of ultra- and super micro pore volume instead of loss of large pores.

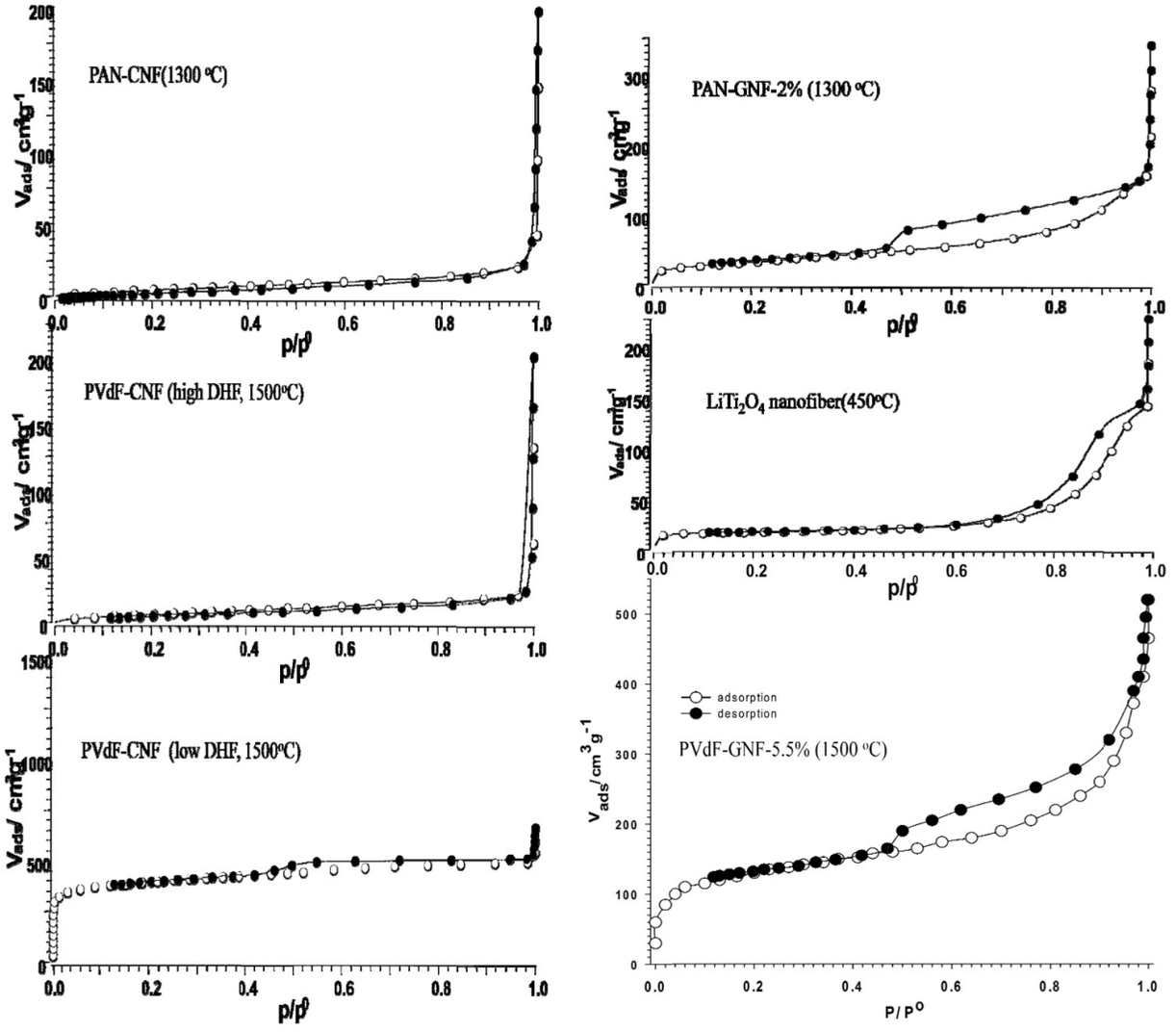

Figure 11. Typical nitrogen adsorption–desorption isotherms for the CNF, GNF and $LiTi_2O_4$ nanofiber prepared from the electrospun nanofibers. in [28] (*These data were reproduced under permissions of The Polymer Society of Korea*)

Samples	Carbonization temperature(°C)		Total pore volume(cm^3/g)	IAA (wt%)	Surface area(m^2/g)	Pore Size Distribution(cm^3/g)			
						< 1 nm[a]	1~2 nm[a]	2~4 nm[b]	4~10 nm[b]
PVdF-CNF	low DHF	800	-	0	967	0.146	0.052	0.075	0.070
		1000	-	0	921	0.166	0.056	0.084	0.101
		1300	-	0	865	0.249	0.065	0.092	0.094
		1500	-	0	414	0.057	0.072	0.103	0.109
		1800	0.63	0	1300	1.767[c]	-	-	-
	high DHF	1000	-	0	33	-	-	0.017	0.014
		1300	-	0	16	-	-	0.006	0.004
		1500	-	0	26	-	-	0.012	0.010
PVdF-GNF		800	0.74	5.5	473	0.162	0.042	0.132	0.294
		1000	0.91	5.5	445	0.158	0.040	0.133	0.315
		1500	1.01	5.5	431	0.143	0.048	0.132	0.186
		1800	2.02	5.5	377	0.115	0.044	0.125	0.180
PAN-CNF		1000	-	0	32	-	-	0.011	0.012
		1300	-	0	22	-	-	0.012	0.012
		1500	-	0	22	-	-	0.008	0.007
PAN-GNF		900	-	2	198	0.048	0.027	0.048	0.039
		1100	-	2	198	0.032	0.024	0.050	0.059
		1300	-	2	60	-	-	0.021	0.046
		1500	-	2	65	0.008	0.007	0.023	0.039
		900	-	5	243	0.044	0.027	0.047	0.060
		1100	-	5	247	0.065	0.030	0.050	0.084
		1300	-	5	116	0.025	0.017	0.040	0.066
		1500	-	5	109	0.030	0.012	0.034	0.056
		1300	-	7.5	163	0.047	0.019	0.041	0.062

[a] determined by applying the Horvath Kawazoe pore sizes for micro porous samples.
[b] determined by applying the B.J.H. pore sizes for meso porous samples.
[c] ultra micro pores of below 0.8 nm

Table 3. Surfacearea and pore analysis of electrospun PVdF- and PAN-based CNFs and GNFs. in [28~31] (These data were reproduced under permissions of The Polymer Society of Korea, Cambridge University Press, and Elsevier)

Samples	Calcinations temperature (°C)	Surface area (m^2/g)	Pore Size Distribution(cm^3/g) (1~2 nm[a])
TiO_2 nanofiber	450	49.4	0.0157
$LiTi_2O_4$ nanofiber	450	50.2	0.0187
$LiTi_2O_4$ nanofiber	700	26.3	0.0090

Table 4. Surface area and pore analysis of electrospun TiO_2 and $LiTi_2O_4$ nanofibers.

2.3. Hydrogen storage capacities

The hydrogen storage capacity of electrospun nanofibrous materials in this chapter was evaluated through the gravimetric method using magnetic suspension balance (MSB, Rubotherm), as show in Figure 12. First, the blank test chamber containing samples was evacuated, to remove the impurities and water, at 150 ^{o}C/10^{-6} torr for 6 hrs. The weights of the sample basket and samples were then measured at 10^{-6} torr/25 ^{o}C (±0.5 ^{o}C) and at a He gas atmosphere of 10 bars, respectively. It was assumed that He gas was not adsorbed by the nanofiber samples in this condition. The weight difference between the vacuum and the 10 bars He gas, which indicates buoyancy due to the He gas, was used to determine the volume of the nanofiber samples, as follows:

$$V_S = W_1/d_{He} \quad (1)$$

where V_S is the volume of the samples, W_1 is the weight difference of the samples between in the vacuum and at the 10-bar He gas atmosphere, and d_{He} is the density of He at a specific pressure and temperature. The weights of the samples were measured under different H_2 pressures (10~100 bars) at 25 ^{o}C (±0.5 ^{o}C). The weights of the absorbed hydrogen were determined after the correction of the buoyancy due to the hydrogen gas atmosphere, using the sample volume (V_S), as follows:

$$\text{The weight of the adsorbed } H_2 = W_2 + V_S\, d_{H2} \quad (2)$$

where W_2 is the weight difference of the samples between in the vacuum and at the specific H_2 pressure, V_S is the volume of the samples, and d_{H2} is the density of H_2 at a specific pressure and temperature. The densities of He and H_2 gas for buoyancy correction were calculated from a real gas equation using the Thermodynamic and Transport Properties of Pure Fluid Program (NIST-supported).

In the case of monolayer condensation of hydrogen on carbon absorbents, theoretical quantity of absorption is 1.3×10^{-5} mol/m^2, in[1,13], and the quantity of reversible hydrogen absorption is known to proportional to specific surface area of absorbents. Commercial active carbons and active carbon fibers generally have very high surface areas of above 1000 m^2/g, and SWNT also has a surface area of a few hundred m^2/g. They showed low storage capacities, however, within the range of 0.35~0.41 wt%, at room temperature, in [7]. Low storage capacity of carbon materials at ambient temperature is due to too low absorption potential between carbon and hydrogen. If the tendency that hydrogen is going to escape from carbon absorbent is smaller than absorption potential, hydrogen will be absorbed as condensed phase by whole micro pore. It is predicted there are the optimum pore size and pore geometry for hydrogen absorption. Therefore, when the kinetic diameter of hydrogen molecule (0.41 nm) is considered, ultra micro pores (< 0.7 nm) are expected by doing important contribution for hydrogen storage by means of nanocapillary mechanism and superposing of potential on the pore wall substantially. Hydrogen adsorption of the CNFs with very low surface area may not be expected because of their low surface area. If they have ultra micro pores, however, which may be effective for hydrogen storage, they will show hydrogen adsorption.

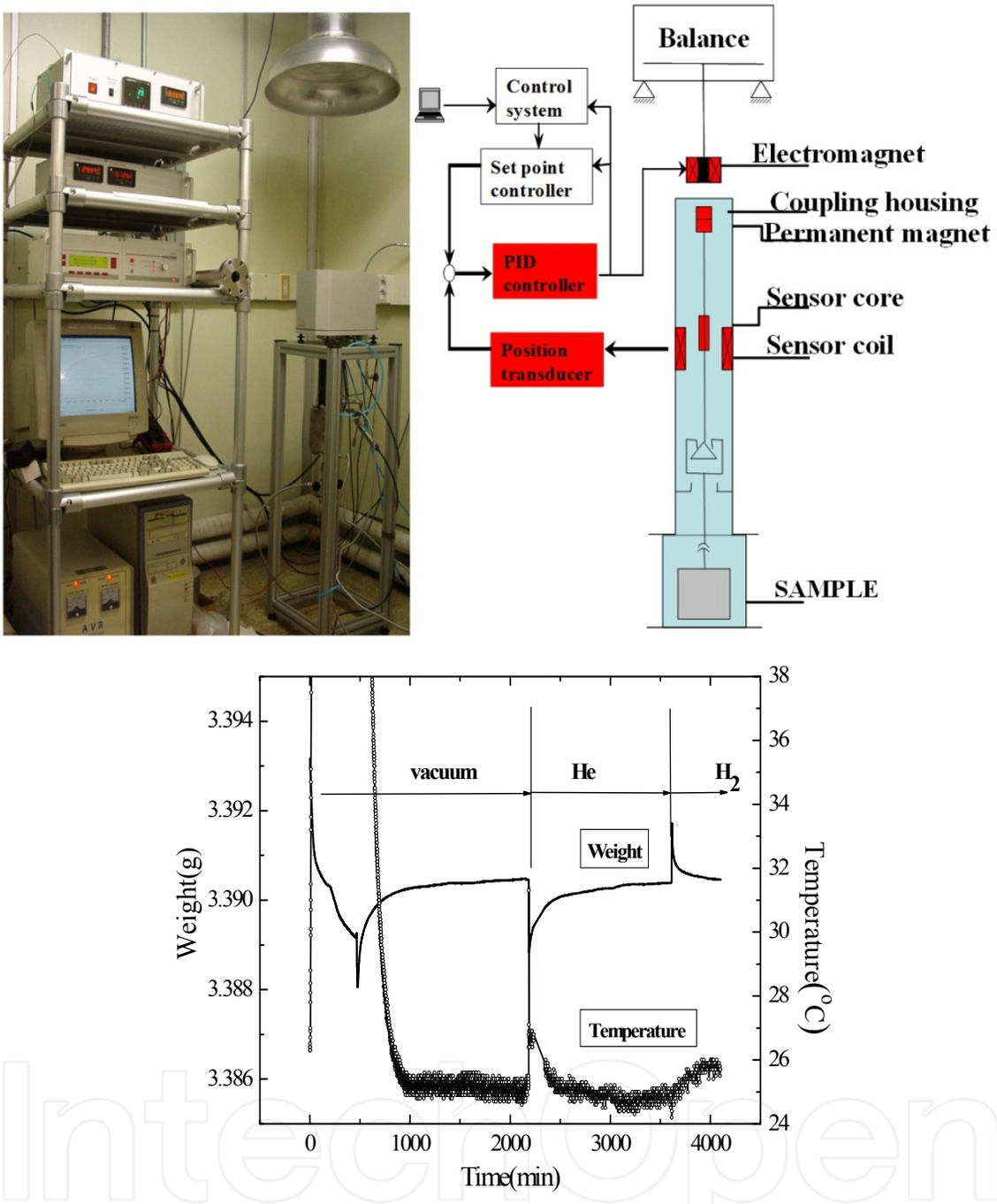

Figure 12. Procedure for evaluation of hydrogen storage by Gravimetric method using Magnetic Suspension Balance.

Figure 13 shows the hydrogen storage results of the electrospun PAN-based CNFs and GNFs under several hydrogen pressures and at room temperature. The hydrogen storage was measured after 2 hrs under a specific hydrogen pressure. Their hydrogen adsorption continuously increased even after 2 hrs, and also increased with increase of hydrogen pressure. The dotted line in Figure 13(a) indicates the increased hydrogen storage capacities after 16 hrs. The hydrogen storage capacities of the PAN-based CNFs obtained from carbonization at 1000°C, 1100 °C and 1300°C, and 1500°C were 0.16 wt%, 0.37 wt%, 0.50 wt%,

and 0.26 wt% respectively, although they were nonporous carbon with very low surface areas in the nitrogen gas adsorption-desorption isotherms. These may indicate the presence of ultra micro pores that cannot differentiate by using nitrogen gas adsorption-desorption isotherms. The reduction of hydrogen storage in the CNF obtained from carbonization at 1500 °C was thought to be due to the disappearance of pore structure including ultra micro pore at high carbonization temperature of above 1300 °C. In the case of the PAN-based GNFs the hydrogen storage capacities increased with increase of carbonization temperature and the content of IAA catalyst, as shown in Figure 13(b), and were higher than those of the CNFs. The hydrogen storages of PAN-based GNF-5 showed highest capacity of 1.01 wt% at 1300 °C and lowest capacity of 0.14 wt% at 1500 °C_similar to those of the PAN based CNF samples. Increase of the content of IAA resulted in increase of the hydrogen storage. The hydrogen storage of the PAN-based GNF-7.5 at 1300 °C, however, showed very low storage of 0.32 wt% though it had higher surface area and higher micro-, meso pore volume than those of GNF-2 and GNF-5 at 1300 °C. So, the hydrogen storage of the PAN-based CNF and GNF did not show the correlation with surface area, and micro-, meso pore volume in Table 3. Fe metal catalyst in the GNFs may contribute to the hydrogen adsorption. Figure 14 showed the cycle property about the hydrogen adsorption of the PAN-based GNF-5 (1300°C), which showed highest storage capacity. The GNF-5 (1300 °C) still retained initial hydrogen capacity storages, indicating physisorption of hydrogen. However, about 0.078 wt% of hydrogen did not desorbed under atmosphere and vacuum of 10^{-6} torr at room temperature. This is thought to be chemisorptions by Fe metal catalyst.

Figure 15 shows the hydrogen storage capacities of the electrospun PVdF-based CNFs. The PVdF-based CNFs (high DHF) also showed some hydrogen absorption although they had no micro pore volumes. The hydrogen absorptions of about 0.3 wt% (100 H_2 bar) were observed in the PVdF-based CNFs (high DHF) prepared at 1,300~1500 °C although they have very low specific surface area of 16~33 m^2/g. But the PVdF-based CNFs (low DHF) prepared at 800~1300 °C showed the hydrogen storage capacities of only 0.05~0.2 wt% in spite of high specific surface area of 865~967 m^2/g. The hydrogen adsorption of the carbon nanofibers with high surface areas decreased with the increase of hydrogen pressure. This may be due to the buoyancy effect of hydrogen gas adsorbed on the samples. Hydrogen storage capacities of the electrospun PVdF-based CNF (low DHF) increased with increase of carbonization temperature and showed the maximum value of about 0.39 wt% at 1500 °C in spite of its lowest surface area. And also the PVdF-based CNF (low DHF) carbonized at 1800 °C showed hydrogen storage capacity of 0.39 wt% even though it had highest surface area of 1300 m^2/g and highest ultra micro pore volume of 1.767 cm^3/g, similar to the activated carbon fibers having 0.35~0.41 wt% hydrogen storage, in [9]. This is thought to be due to the disappearance of the pore structure including ultra micro pores at high carbonization temperatures. Figure 16 shows hydrogen storage results for the PVdF-based GNFs under several hydrogen pressures at room temperature. Their hydrogen adsorption increased with increase of carbonization temperature while specific surface area and micro pore volume (< 1 nm) were decreased, but they showed very low storage capacities of about 0.1~0.2 wt% although they have highly graphite crystalline structure.

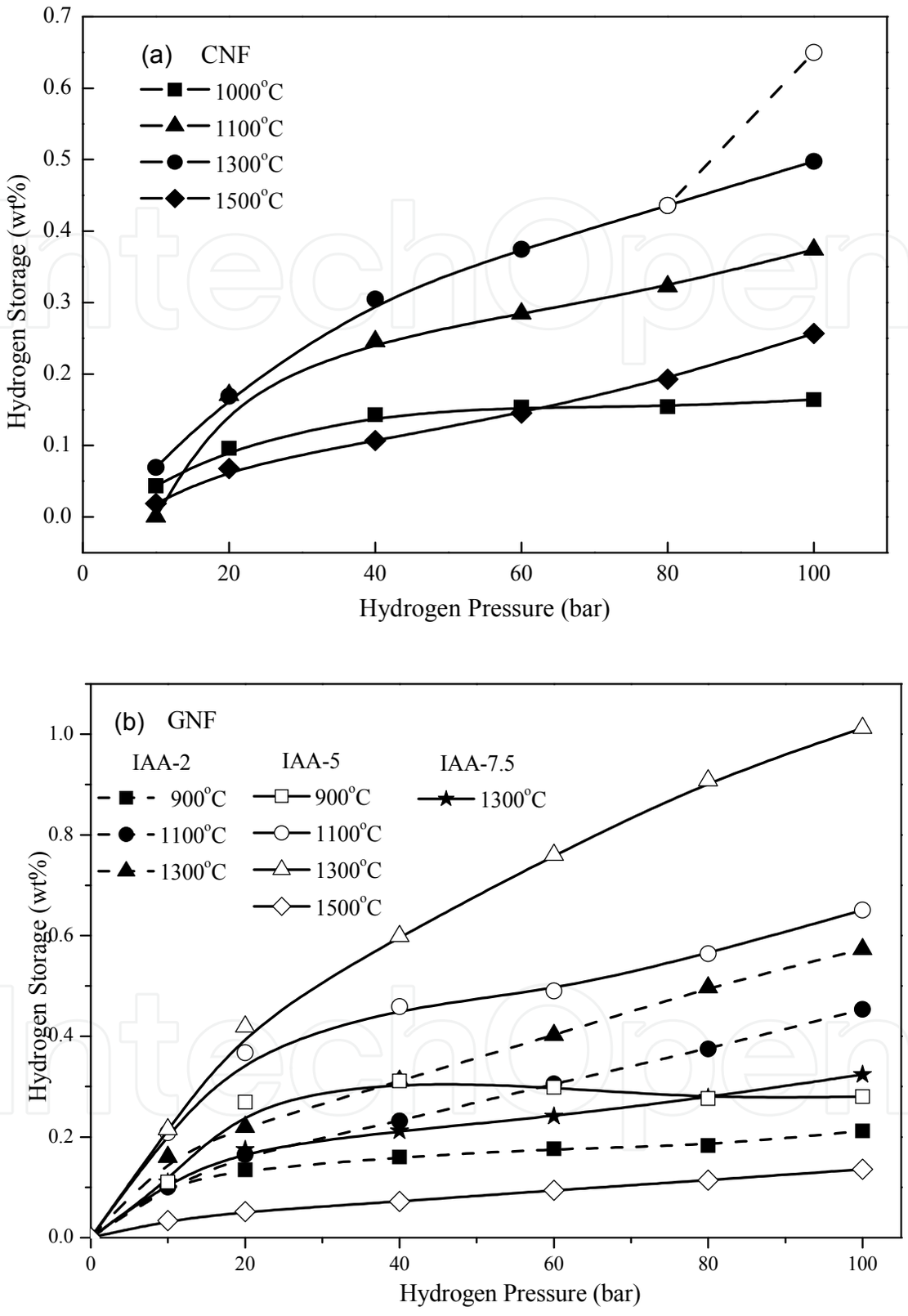

Figure 13. The hydrogen storage of the PAN-based (a) CNFs and (b) GNFs under several hydrogen pressures and at room temperature. in [28,29] (*These data were reproduced under permissions of The Polymer Society of Korea and Cambridge University Press*)

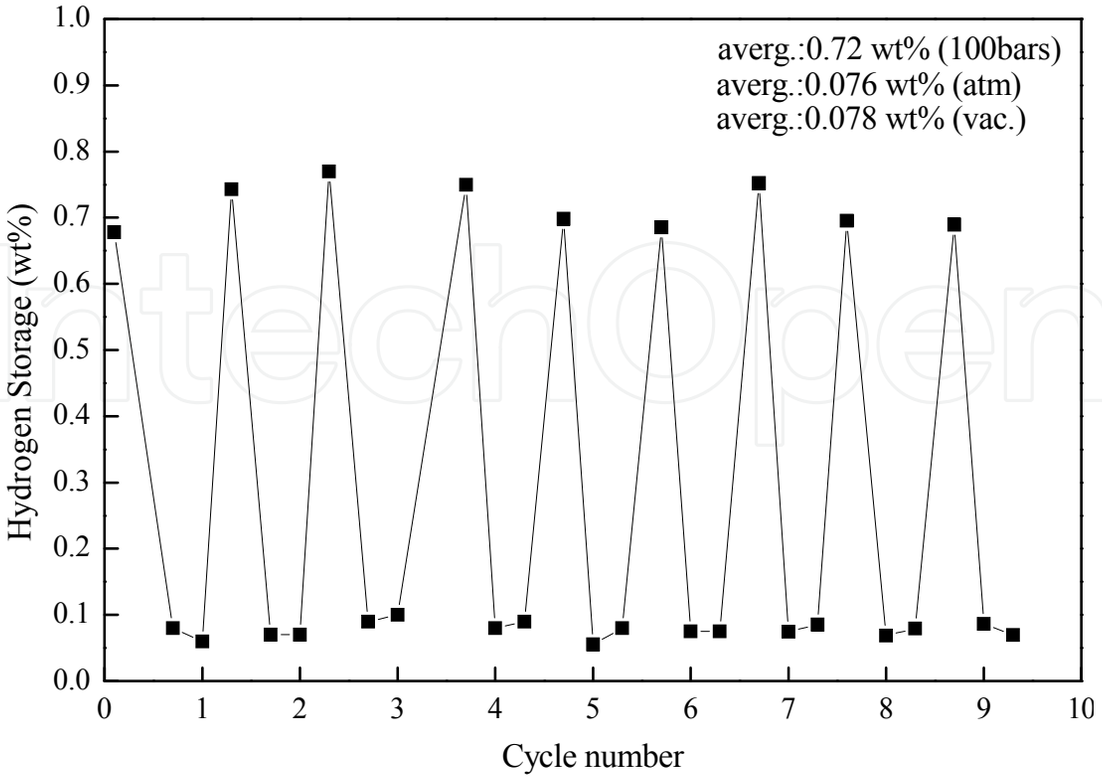

Figure 14. The hydrogen adsorption/desorption cycle property of the PAN-based GNF-5 (1300°C) under hydrogen pressures of 100 bars and at room temperature. in [28] (*These data were reproduced under permissions of The Polymer Society of Korea*)

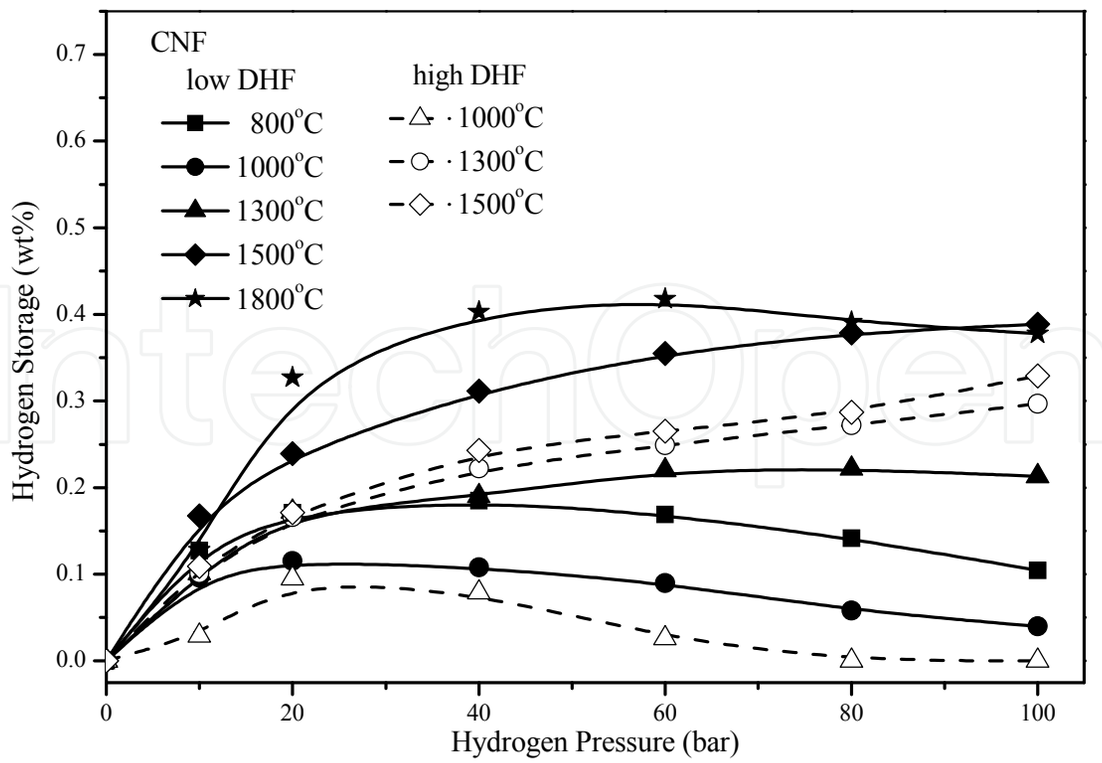

Figure 15. The hydrogen storage of the PVdF-based CNFs under several hydrogen pressures and at room temperature. in [30] (*These data were reproduced under permissions of Cambridge University Press*)

The hydrogen storage capacity of the GNFs and CNFs did not show correlation with surface area or micro- and meso pore volume, as shown in Table 3**.** The quantity of adsorbed hydrogen on nanostructure graphitic carbon as well active carbon materials at 77 K is proportional to the specific surface area of carbon materials, in [10]. However, because at ambient temperature the thermal motion of hydrogen molecules overcomes van der Waals-type weak physisorption of molecular hydrogen, their hydrogen storage capacities were very low. So the hydrogen adsorption on the GNFs and CNF samples may be influenced by pore structure as well as specific surface area. Therefore, we think that micro- and meso pores that are calculated using the nitrogen gas adsorption–desorption isotherms are not the effective pore for hydrogen storage. The effective pore for hydrogen storage may require small pore size not exceeding 1 nm, when compared to the kinetic diameter of hydrogen molecule of about 0.41 nm. It is assumed that these micro pores are different from the micro pores calculated using nitrogen adsorption–desorption isotherms. Thus, hydrogen adsorptions by the electrospun PAN or PVdF-based CNFs and GNFs may be due to the presence of ultra micro pores rather than micro- and meso pores, even though they have very low surface areas compared to commercially available active carbons and active carbon fibers.

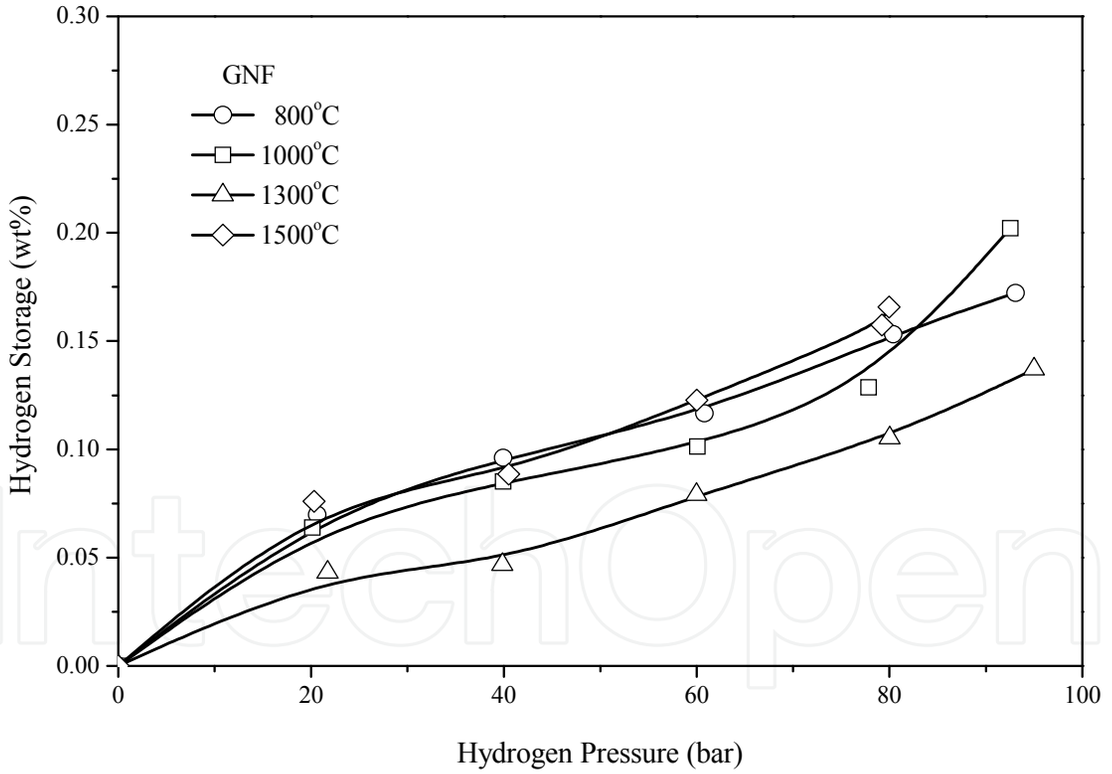

Figure 16. The hydrogen storage of the PVdF-based GNFs under several hydrogen pressures and at room temperature. in[31] (*These data were reproduced under permissions of Elsevier)*

The multilayered TiO_2 nanotubes with a surface area of 199 m^2/g (a pore size; 8 nm, and a pore volume; 0.70 cm^3/g) had known to store a 1~2.5 wt% hydrogen at 1 bar and room temperatures in the range 80 to 125 °C, in [13]. This high storage capacity may result from much higher adsorption potential energy between the multilayered TiO_2 nanotubes and

hydrogen molecules than those of carbon materials in consideration of very low hydrogen storage of typical meso porous carbon materials with high surface area. Figure 17 shows hydrogen storage results for the electrospun TiO_2 nanofiber and $LiTi_2O_4$ nanofibers. The hydrogen storage was measured after 2 hrs under a specific hydrogen pressure. The TiO_2 nanofiber and $LiTi_2O_4$ nanofibers calcined at 450 ^oC showed high hydrogen storages of 1.11 wt% and 0.74wt% in spite of their low surface area of 49.4 m^2/g and 50.2 m^2/g, respectively. Their hydrogen absorptions were higher than those of the electrospun CNFs and GNFs. Although we presently cannot determine effective ultra micro pore volumes for hydrogen storage in the TiO_2 nanofiber and $LiTi_2O_4$ nanofibers, these are thought to be due to higher adsorption potential energy between the metal oxide materials and hydrogen molecules than those of carbon nanofibers. The $LiTi_2O_4$ nanofiber showed higher hydrogen storage than TiO_2 nanofiber with similar surface area. This is also thought to be due to higher adsorption potential energy of $LiTi_2O_4$ nanofiber than TiO_2 nanofiber. The hydrogen storage of the $LiTi_2O_4$ nanofiber calcined at 700 ^oC was greatly reduced to 0.41 wt%. Increase of the calcination temperature resulted in decrease of hydrogen storage with great reduction of surface area, indicating loss of effective pores with increase of $LiTi_2O_4$ crystalline size, as shown in Figure 9. Figure 18 showed the hydrogen adsorption/desorption cycle of electrospun $LiTi_2O_4$ nanofibers. Their hydrogen adsorption continuously increased even after 2 hrs under hydrogen pressure of 100 bars. The hydrogen storage of the $LiTi_2O_4$ nanofibers calcined at 450^{o}C and 600^{o}C were about 1.50wt% and 1.23 wt% at the equilibrium state under hydrogen pressure of 100 bars, respectively. However, about 0.06 wt% and 0.054 wt% of hydrogen were not desorbed under atmosphere and vacuum of 10^{-6} torr at room temperature, respectively. These are thought to be chemisorptions.

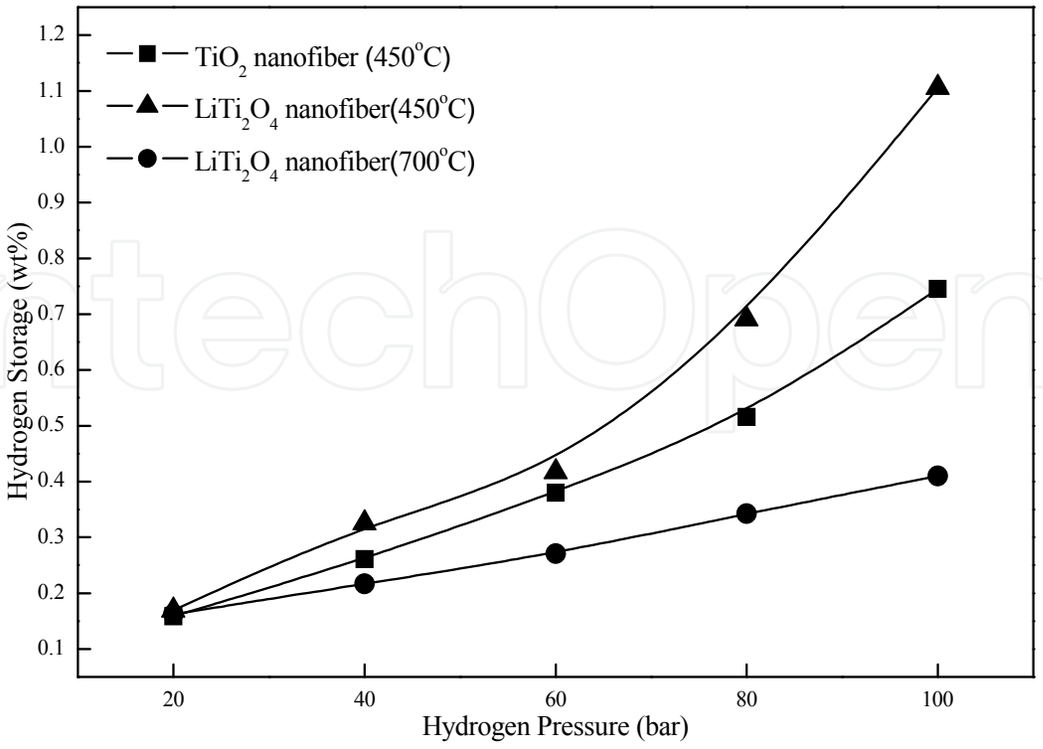

Figure 17. The hydrogen storage capacity of the electrospun TiO_2 nanofiber and $LiTi_2O_4$ nanofibers.

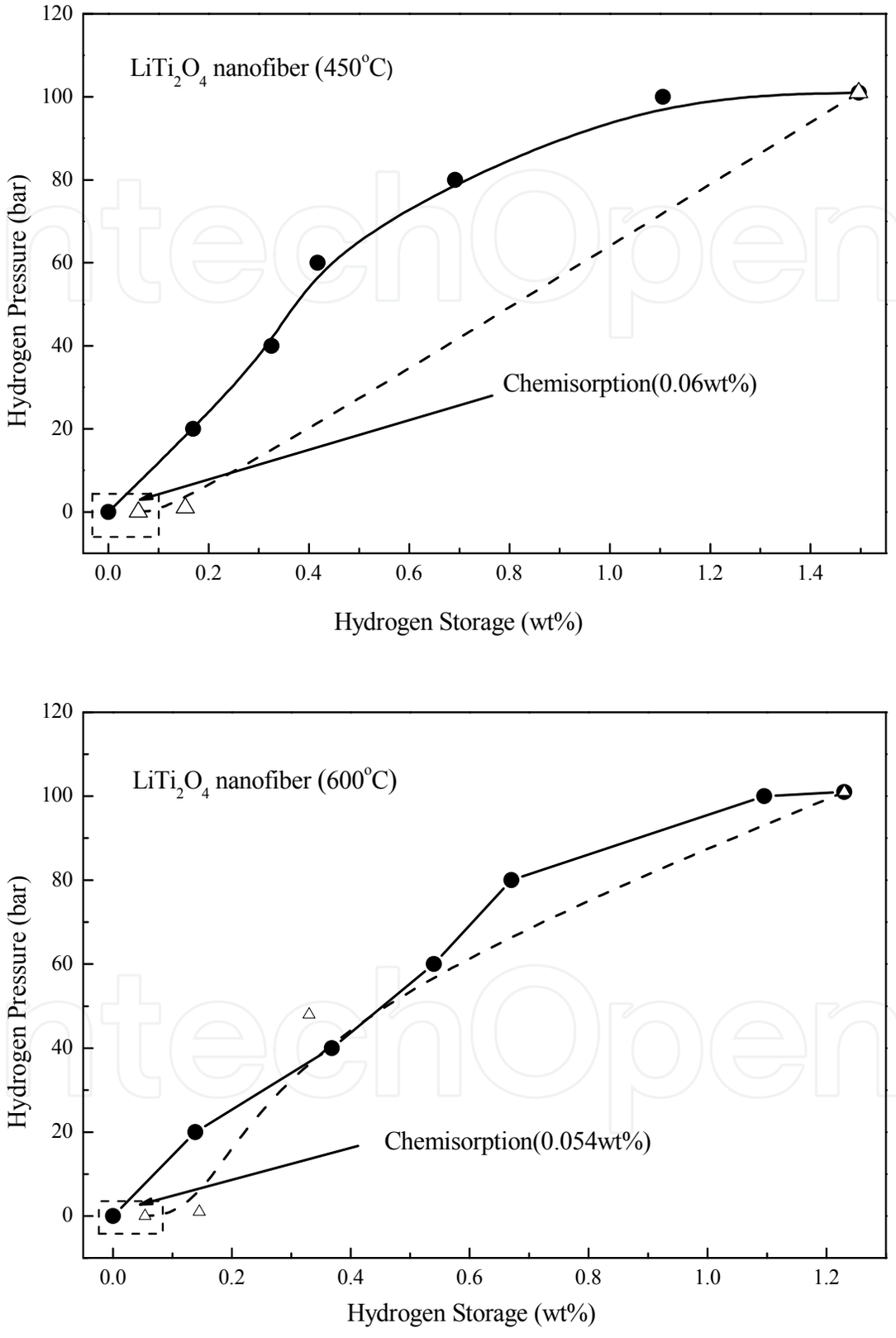

Figure 18. The hydrogen adsorption/desorption cycle of the electrospun $LiTi_2O_4$ nanofibers under hydrogen pressures of 100 bars and at room temperature.

2.4. Further work

Active carbon with the same specific surface area reversibly adsorbed 2 mass% hydrogen at a temperature of 77 K, in [1,2]. The quantity of adsorbed hydrogen on nanostructured graphitic carbon as well active carbon materials at 77 K is proportional to the specific surface area of carbon materials, in [10]. However, because at ambient temperature the thermal motion of hydrogen molecules overcomes van der Waals-type weak physisorption of molecular hydrogen, high surface area and large micro- and meso pores volumes of active carbon does not greatly contribute to the hydrogen adsorption. The effective pores for hydrogen storage are assumed to be ultra micro pores with small pore size not exceeding 1 nm, when compared to the kinetic diameter of hydrogen molecule of about 0.41 nm. The electrospun CNF and GNF were prepared by carbonization without further activation process to induce increase of ultra micro pore through heat-treatment for densification of large pores structure at high temperature. Thus, hydrogen adsorptions results of the electrospun CNFs and GNFs indicated the presence of ultra micro pores even though they have very low surface area and micro-, meso pores, that are calculated using the nitrogen gas adsorption–desorption isotherm, when compared to commercially available active carbons or active carbon fibers. For automotive and industrial applications, the solid absorbent with hydrogen storage capacity of greater than 6.5 wt% and ambient temperatures for hydrogen release are presently required. The hydrogen storage capacities of the electrospun CNFs and GNFs, however, still showed the limitations in overcoming this requirement. That is, it may not be possible to increase effective ultra micro pores for above 6.5 wt% hydrogen storage even though we can find more improved process for the CNF and GNF in future.

On the other hands, the hydrogen storage results in TiO_2 nanofiber and $LiTi_2O_4$ nanofibers gave to some encouragement for overcoming hydrogen storage target. They showed 1.2~1.5 wt% hydrogen in spite of very low surface area of about 50 m^2/g. These were higher than those of the electrospun CNFs and GNFs because the TiO_2 nanofiber and $LiTi_2O_4$ nanofibers are thought to be due to higher adsorption potential energy between the metal oxide materials and hydrogen molecules than those of carbon nanofibers. So, future works for the high hydrogen storage capacity need new solid absorbent materials with a high ultra micro pore volume, high surface area, and appropriate hydrogen adsorption potential energy for only reversible physisorption.

Therefore, further work for this purpose will be tried to prepare new nanostructures metal oxide nanofibers with high reversible physisorption at ambient temperature, which are controlled to a high surface area and high ultra micro pore volumes.

3. Conclusions

The hydrogen storage capacities of electrospun nanofibrous materials were discussed in view of their pore size, surface area, and adsorption potential energy for hydrogen molecules. Carbon nanofibers (CNF) and graphite nanofibers (GNF) were prepared through the carbonization of the electrospun PAN- and PVdF-based nanofibers. The TiO_2 nanofiber and $LiTi_2O_4$ were also prepared through typical electrospinning of precursor solutions.

The hydrogen storage capacities of the PAN-based CNFs prepared by carbonization at 1000 °C, 1100 °C and 1300°C, and 1500°C were 0.16 wt%, 0.37 wt%, 0.50 wt%, and 0.26 wt% respectively, although they were nonporous carbon with very low surface areas of about 22~32 m^2/g in the nitrogen gas adsorption-desorption isotherms. The PVdF-based CNFs (high DHF) prepared by carbonization at 1300°C and 1500°C showed very low surface area of about 16~26 m^2/g without the micro pores and showed the adsorption curves similar to those of nonporous carbon in nitrogen gas adsorption-desorption isotherms. However, they also stored the hydrogen of 0.30 wt% and 0.33 wt%, respectively.

The PAN-based GNFs had some micro-, meso pores and higher surface areas of 60~253 m^2/g than the CNFs though they were still much lower surface area compared to common active carbon. Their surface area decreased with increase of carbonization temperature and increased with increase of IAA content. Although this could not be fully explained at present, it may be due to the surface roughness and inhomogeneous structure of the GNFs, which resulted from the induction of the metal catalyst in the GNFs. The hydrogen storage capacities of them increased with increase of carbonization temperature and the content of IAA catalyst, and were higher than those of the CNFs. The hydrogen storages of PAN-based GNF-5 showed highest capacity of 1.01 wt% at 1300 °C and lowest capacity of 0.14 wt% at 1500 °C.

The PVdF-based CNFs (low DHF) showed typical curves of micro porous carbon in the nitrogen gas adsorption-desorption isotherms. They had high surface areas of 414~1300 m^2/g and stored the hydrogen of 0.04-0.39 wt%. The PVdF-based CNF (low DHF) at 1800 °C showed the hydrogen storage of only 0.38 wt% in spite of high surface area of 1300 m^2/g and a high volume (1.767 cm^3/g) of only ultra- or super micro pores. Nitrogen adsorption–desorption isotherms for the PVdF-based GNFs prepared from carbonization at 800~1800°C were the type II showing a hysteresis loop that indicates the existence of meso pores. They had high surface areas of 377~473 m^2/g but showed very low storage capacities of about 0.1~0.2 wt% although they have highly graphite crystalline structure.

The above hydrogen storage capacities of the GNFs and CNFs did not show any correlations with surface area or micro- and meso pore volume calculated using nitrogen adsorption–desorption isotherms. Because at ambient temperature the thermal motion of hydrogen molecules overcomes van der Waals-type weak physisorption of molecular hydrogen, their hydrogen storage capacities were very low. So the hydrogen adsorption on the GNFs and CNF samples may be influenced by pore structure as well as specific surface area. Therefore, micro- and meso pores that are calculated using the nitrogen gas adsorption–desorption isotherms are not thought to be the effective pore for hydrogen storage. The effective pore for hydrogen storage may require small pore size not exceeding 1 nm, when compared to the kinetic diameter of hydrogen molecule of about 0.41 nm. Thus, hydrogen adsorptions by the electrospun PAN or PVdF-based CNFs and GNFs may be due to the presence of ultra micro pores rather than micro- and meso pores, even though they have very low surface areas compared to commercially available active carbons and active carbon fibers.

The TiO_2 nanofiber and $LiTi_2O_4$ nanofibers calcined at 450 ^oC showed high hydrogen storages of 1.11 wt% and 0.74wt% in spite of their low surface areas of 49.4 m^2/g and 50.2 m^2/g, respectively. Their hydrogen storages were higher than the electrospun CNFs and GNFs. Although we presently cannot determine the effective ultra micro pore volumes for hydrogen storage, their high hydrogen adsorptions are thought to be due to higher adsorption potential energy than those of carbon nanofibers. The hydrogen storage of $LiTi_2O_4$ nanofiber was higher than that of TiO_2 nanofiber with similar surface area, indicating higher adsorption potential energy of $LiTi_2O_4$ nanofiber than that of TiO_2 nanofiber. So, the high hydrogen storage capacity need new solid absorbent materials with a high ultra micro pore volume, high surface area, and appropriate hydrogen adsorption potential energy for only reversible physisorption at ambient temperature.

Author details

Seong Mu Jo
Center for Materials Architecturing, Korea Institute of Science and Technology, Seoul, Republic of Korea

4. References

[1] Schlapbach L and Zuttel A, (2001), Hydrogen-Storage Materials for Mobile Applications, Nature, 414: 353-358.

[2] Nellis, W. J, Louis, A. A, and Ashcroft, N. W, (1998), Metallization of fluid hydrogen. Phil. Trans. R. Soc. Lond. A356: 119-135

[3] Dillon A. C, Jones K. M, Bekke-dahl T. A., Kiang H, Bethune D. S, and Heben M. J, (1997), Storage of Hydrogen in Single-Walled Carbon Nanotubes, Nature, 386: 377-379.

[4] Zhu H, Cao A, Li X, Xu C, Mao Z, Ruan D, Liang J, and Wu D, (2001), Hydrogen Adsorption in Bundles of Well-Aligned Carbon Nanotubes at Room Temperature, Appl. Surf. Sci., 178: 50-55.

[5] Ye Y, Ahn C. C, Witham C, Fultz B, Liu J, Rinzler A. G, Colbert D, Smith K. A, and Smalley R. E, (1999), Hydrogen Adsorption and Cohesive Energy of Single-Walled Carbon Nanotubes, Appl. Phys. Lett.,74: 2307-2309.

[6] Liu C, Fan Y. Y, Lyu M, Cong H. T, Cheng H. M, and Dresselhaus M. S, (1999), Hydrogen Storage in Single-Walled Carbon Nanotubes at Room Temperature, Science, 286: 1127-1129.

[7] Liu C, Yang Q. H, Tong Y, Cong H. T., and Chen H. M, (2002), Volumetric Hydrogen Storage in Single-Walled Carbon Nanotubes, Appl. Phys. Lett., 80: 2389-2391

[8] Quinn D. F, (2002), Supercritical Adsorption of 'Permanent' Gases under Corresponding States on Various Carbons, Carbon, 40: 2767-2773.

[9] Kajiura K, Tsutsui S, Kadona K, and Ata M, (2003), Hydrogen Storage Capacity of Commercially Available Carbon Materials at Room Temperature, Appl. Phys. Lett., 82: 1105-1107.

[10] Nijkamp M. G, Raaymakers J. E. M. J, Van Dillen A. J, and de Jong K. P, (2001), Hydrogen Storage using Physisorption-Materials Demands, Appl. Phys., A, 72: 619-623.
[11] Chahine R and Bose T. K, (1994), Low-pressure Adsorption Storage of Hydrogen, Int. J. Hydrogen Energy, 19: 161-164.
[12] Lim S. H, Luo J, Zhong Z, Ji W, and Lin J, (2005), Room-Temperature Hydrogen Uptake by TiO_2 Nanotubes, Inorg. Chem., 44: 4124-4126.
[13] Bavykin D. V, Lapkin A. A, Plucinski P. K, Friedrich J. M., and Walsh F. C, (2005), Reversible Storage of Molecular Hydrogen by Sorption into Multilayered TiO_2 Nanotubes, J. Phys. Chem. B 109: 19422-19427.
[14] Wan Q, Lin C. L, Yu X. B, and Wang T. H, (2004), Room-Temperature Hydrogen Storage Characteristics of ZnO Nanowires, Appl. Phys. Lett., 84 (1): 124-126.
[15] Chen J, Kuriyama N, Yuan H, Takeshita H. T, and Sakai T, (2001), Electrochemical Hydrogen Storage in MoS_2 Nanotubes, J. Am. Chem. Soc., 123: 11813-11814.
[16] Chen J, Li S.-L., Tao Z.- L, Shen Y.- T, and Cui C.- X, (2003), Titanium Disulfide Nanotubes as Hydrogen-Storage Materials J. Am. Chem. Soc., 125: 5284-5285.
[17] Yamashita J, Shioya M, Kikutani T, and Hashimoto T, (2001), Activated Carbon Fibers and Films Derived from Poly(vinylidene fluoride), Carbon, 39: 207-214.
[18] Choi S. W, Jo S. M, Lee W. S, and Kim Y. R, (2003), An Electrospun Poly(vinylidene fluoride) Nanofibrous Membrane and Its Battery Applications, Adv. Mater, 15(23): 2027-2032.
[19] Kim J. R, Choi S. W, Jo S. M, Lee W. S, and Kim B. C, (2005), Characterization and Properties of PVdF-HFP-Based Fibrous Polymer Electrolyte Membrane Prepared by Electrospinning, J. Electrochem. Soc., 152(2): A295-A300
[20] Choi S. W, Kim J. R. Jo S. M. Lee W. S. and Kim Y.-R. (2005), Electrochemical and Spectroscopic Properties of Electrospun PAN-Based Fibrous Polymer Electrolytes, J. Electrochem. Soc., 152(5), A989-A995.
[21] Song M. Y, Kim D. K, Ihn K. J, Jo S. M., and Kim D. Y, (2004), Electrospun TiO_2 Electrodes for Dye-Sensitized Solar Cells, Nanotechnology, 15 : 1861-1865.
[22] Song M. Y, Ahn Y. R, Jo S. M , Ahn J-. P, and Kim D. Y, (2005), TiO_2 Single-Crystalline Nanorod Electrode for Quasi-Solid State Dye-Sensitized Solar Cells, Appl. Phys. Lett., 87: 113113-1~113113-3.
[23] Kaburagi Y, Hishiyama Y, Oka H, and Inagaki M, (2001), Growth of Iron Clusters and Change of Magnetic Property with Carbonization of Aromatic Polyimide Film Containing Iron Complex, Carbon, 39: 593-603.
[24] Konno H, Shiba K, Kaburagi Y, Hishiyama Y, and Inagaki M, (2001), Carbonization and Graphitization of Kapton-type Polyimide Film having Boron-bearing Functional Groups, Carbon, 39: 1731-1740.
[25] Reshetenko T. V, Avdeeva L. B, Ismagilov Z. R, Pushkarev V. V, Cherepanova S. V, Chuvilin A. L, and Likholobov V. A, (2003), Catalytic Filamentous Carbon Structural and Textural Properties, Carbon, 41: 1605-1615.
[26] Chung G. S, Jo S. M, and Kim B. C, (2005), Properties of Carbon Nanofibers Prepared from Electrospun Polyimide, J. Appl. Polym. Sci., 97: 165-170.

[27] Park S. H, Jo S. M, Kim D. Y, Lee W. S, and Kim B. C, (2005), Effects of Iron Catalyst on the Formation of Crystalline Domain during Carbonization of Electrospun Acrylic Nanofiber, Syn. Met., 150: 265-270.

[28] Kim D.- K, Park S. H, Kim B. C, Chin B. D, Jo S. M, and Kim D. Y, (2005), Electrospun Polyacrylonitrile based Carbon Nanofibers and Their Hydrogen Storage, Macromolecular Research, 13(6): 521-528.

[29] Park S. H. Kim B. C. Jo S. M. Kim D. Y. and Lee W. S. (2005), Cabon Nanofibrous Materials Prepared from Electrospun Polyacrylonitrile Nanofibers for Hydrogen Storage, Mater. Res. Soc. Symp. Proc., 837: 71-76

[30] Chung H. J, Lee D. W, Jo S. M, Kim D. Y, and Lee W. S, (2005), Electrospun Poly(vinylidene fluoride)-based Carbon Nanofibers for Hydrogen Storage, Mater. Res. Soc. Symp. Proc., 837: 77-82

[31] Hong S. E, Kim D.- K., Jo S. M, Kim D. Y, Chin B. D, Lee D. W, (2007), Graphite Nanofibers Prepared from Catalytic Graphitization of Electrospun Poly(vinylidene fluoride) Nanofibers and Their Hydrogen Storage Capacity, Catalysis Today, 120(3-4): 413-419

[32] Hishiyama Y, Igarashi K, Kaneko I, Fujii T, Kaneda T, Koidezawa T, Shimazawa Y, and Yoshida A, (1997), Graphitization Behavior of Kapton-derived Carbon Film Related to Structure, Microtexture and Transport Properties, Carbon, 35: 657-668.

[33] Ra W, Nakayama M, Uchimoto Y, and Wakihara M, (2005), Experimental and Computational Study of the Electronic Structural Changes in $LiTi_2O_4$ Spinel Compounds upon Electrochemical Li Insertion Reactions, J. Phys. Chem. B, 109(3): 1130-1134.

[34] Manickam M, Takata M, (2003), Lithium Intercalation Cells $LiMn_2O_4/LiTi_2O_4$ without Metallic Lithium, J. Power Sources, 114: 298-302.

[35] Inagaki M, (2000), Control of structure and functions, in New Carbons : Elsevier Science Ltd., chapt. 4- 5.